Column base plates under biaxial bending moment and axial force

L. da Silva Seco, Maël Couchaux, Mohammed Hjiaj, L. Costa Neves

Version of Record: https://www.sciencedirect.com/science/article/pii/S0141029621010439
Manuscript_98a712e50c7c99cbfd93ab48055ea57b

COLUMN BASE PLATES UNDER BIAXIAL BENDING MOMENT AND AXIAL FORCE

Laura DA SILVA SECO[1], Maël COUCHAUX[1,*], Mohammed HJIAJ[1], Luis COSTA NEVES[2]

[1] Structural Engineering Research Group / LGCGM
INSA de Rennes / UEB
20 avenue des Buttes de Coësmes
F – 35708 Rennes
FRANCE

[2] INESCC, Civil Engineering Departement
University of Coimbra,
Coimbra
PORTUGAL

* Corresponding author: Email: mael.couchaux@insa-rennes.fr
Fax: + 33 2 23 23 82 24

Abstract

This paper deals with an extensive finite element parametric study on exposed column base plates subjected to the combination of biaxial bending moment and axial force. The objective is to explore the effect of the connection geometry as well as loading conditions on the resistance and rotational stiffness of the base-plate connection. The influence of the base plate thickness, anchor bolt diameter, column cross section (I or H section), bending moment orientation and axial force magnitude is investigated in details using a numerical model that has been previously validated based on experimental tests performed by the authors. A particular attention is dedicated to the contact pressure distribution and the M-N interaction curves. Analytical models are proposed to evaluate the in-plane, out-of-plane and biaxial bending resistances considering the contribution of an axial force. Both the contribution of the column web and the size of the compression area depend on the base-plate thickness and are accounted for in the evaluation of the in-plane bending resistance. For out-of-plane bending resistance, a parabolic M-N interaction curve is derived. The biaxial bending resistance is evaluated considering the plastic redistribution of out-of-plane bending moments between the right and the left sides of the column base plate (with respect to the strong axis). A simplified method is also proposed to determine the resistance whatever the orientation of the bending moment and the axial force.

1. INTRODUCTION

Column base plates are key components of steel structures as they transfer vertical and horizontal loadings from the building to the foundation. Pinned column base-plates are often used in buildings due to simplicity of execution and the economy. Semi-rigid or rigid column base plates are useful to limit lateral displacements caused by wind or horizontal seismic actions, particularly when the displacement limit is constrained by the presence of overhead crane, for example. A large number of design methods found in the literature address the case of combined axial force and in-plane bending moment. The first generation of design codes were based on an elastic analysis of column base plates ([1], [2]) assuming a linear distribution of contact pressure between the base-plate and the concrete block. This assumption is retained in the brand new standard dedicated to mechanical fasteners, Eurocode 2 part 4 [3]. However, this elastic linear distribution of contact pressure over the entire area of the base plate is realistic for relatively large base-plate thickness only, a situation that is not common in practice. Furthermore, the actual contact pressure distribution between concrete and base-plate is far more complex than what has been assumed.

A large amount of research focused on the development of methods that consider plastic distribution of contact pressure between the base plate and concrete ([4], [5], [6], [7]). These concepts have been introduced in the last generation of design codes for column base-plates ([8], [9]). The above mentioned researchs and design codes deal with the case of column base-plates under strong axis in-plane bending moment combined with an axial force. However, many column base plates are subjected to the combination of a biaxial bending moment and an axial force mainly due to the bidirectional nature of wind and seismic loads. Recently, experimental and numerical studies have been performed to better understand the behavior of column base plates under biaxial bending moment and axial force. Lee et al [10] performed the first experimental tests on column base plates subjected to weak axis bending moment. The failure of the connections was due to column flange yielding/buckling and weld tearing and didn't involve connections components such as anchor bolts or base plate in bending. These results cannot be used to calibrate an analytical model that provide the resistance of the column base

plate for out-of-plane bending moment. The numerical studies performed by Lee et al. [11] on column base plates under out-of-plane bending moment highlighted that the application of the Drake and Elkin approach [5] is not adequate for this case. The first experimental program performed on column base plates subjected to an axial force combined with a biaxial bending moment was carried out by Bajer et al. [12]. This study allowed to evaluate the influence of the orientation of the bending moment axis on the bending resistance and initial rotational stiffness. Under biaxial bending moment, the moment resistance and rotational stiffness were below than the corresponding values under strong axis bending moment alone. The failure mode that corresponds to anchor bolt rupture in tension was not affected by the orientation of the bending moment axis. However, the mechanical characteristics of steel material were not provided, preventing any calibration. Amaral [13] modelled the abovementioned column base plate tests with the finite element code Abaqus and the results were in good agreement. An analytical model based on the component method was proposed to estimate the resistance and initial stiffness in presence of axial force and out-of-plane bending moment. For dominant out-of-plane bending moment, the extent of the compression area depends on the axial force and the resistance of the tensile area. The connection resistance under biaxial bending moment was modelled by a simple elliptical interaction curve and the results were found to be quite conservative compared to experimental and numerical ones. The same approach was adopted by Fasaee et al. [14] whom proposed an analytical model to characterize the resistance of base-plates under axial force and biaxial bending moment, based on an elliptical interaction curve. Results were confirmed by the extensive numerical study. Nevertheless, these elliptical interaction curves does not rely on firm mechanical background. The present authors [18] performed six experimental tests on column base plates subjected to uniaxial (in-plane and out-of-plane) and biaxial bending moments considering two base-plate thicknesses (thin and thick). The failure mode corresponding to anchor bolt rupture in tension with and without base-plate yielding was not affected by the orientation of the bending moment axis. Under biaxial bending moment, the developed finite element model highlighted the dependency of the contact pressure distribution on the base plate thickness and the plastic redistribution between anchor bolts. An analytical model considering this latter observation was proposed to evaluate the uniaxial and biaxial bending resistances. However, this study neglected the presence of axial force

that is crucial for this type of connection. The objective of this paper is thus to develop an analytical model, based on mechanical principles, to determine the resistance of column base plates subjected to the combination of biaxial bending moment and axial force.

This paper presents in section 2 results of an extensive finite element parametric study performed on column base plates subjected to axial force and biaxial bending moment. The numerical model, developed in the finite element code Abaqus and previously validated by comparing its predictions against experimental test results [18] will be used to broaden the results data base. This parametric study shade the light on the influence of the base plate thickness, the column steel profile (I or H section), the diameter of anchor bolts, the orientation of the bending moment axis and the magnitude of the axial force. A particular attention is dedicated to the contact pressure distribution, bending resistance and rotational stiffness. The interaction curves are presented for different orientations of the bending moment axis. Analytical models are proposed to evaluate the uniaxial and biaxial bending resistances. A particular attention is dedicated to the evaluation of the size of the compressive area as a function of the base plate thickness, in the same way Eurocode 3 does. For in-plane bending moment, the contribution of the column web in the compressive area is considered. The component "column in compression" is directly integrated in the evaluation of the resistance of the compressive area. For out-of-plane bending moment, a parabolic interaction curve is derived from equilibrium. Finally, the plastic redistribution observed numerically is integrated in the model for the connection resistance under biaxial bending moment. The results of the proposed analytical models are compared to experimental and numerical data's. A simple equation is finally proposed to estimate the bending resistance whatever the orientation of the bending moment and the value of the axial force.

2. PARAMETRIC STUDY

2.1. Introduction

A finite element model for column base plates subjected to biaxial bending moment and axial force has been developed in Abaqus by the authors ([17], [18]). The results of this model were in very good agreement with those of six experimental tests [18] performed on column base plate subjected to in-plane, out-of-plane and bi-axial bending moments but without axial force. A parametric study on column base plates has been accomplished to enlarge the set of results covering cases that have not been considered yet and to investigate the effects of the base-plate thickness t_p, the shape of the column steel profile (HEA or IPE), the diameter of anchor bolts and the arrangement of the anchoring system. The response of the connection is evaluated for a combination of tensile/compressive axial force and bending moment (in-plane, out-of-plane and biaxial). In particular, the influence of the loading conditions on the failure mode is carefully analyzed. The specimen geometries considered for the parametric study are based on connections tested by the authors [18].

2.2. Finite element model

All components (base-plate, column, weld, concrete, anchor bolts …) except the reinforcing bars are modelled as three-dimensional deformable solids using eight-node linear brick elements (see Fig. 1-a and b). Two-node linear truss elements are used for the concrete reinforcing bars (see Fig. 1-c).

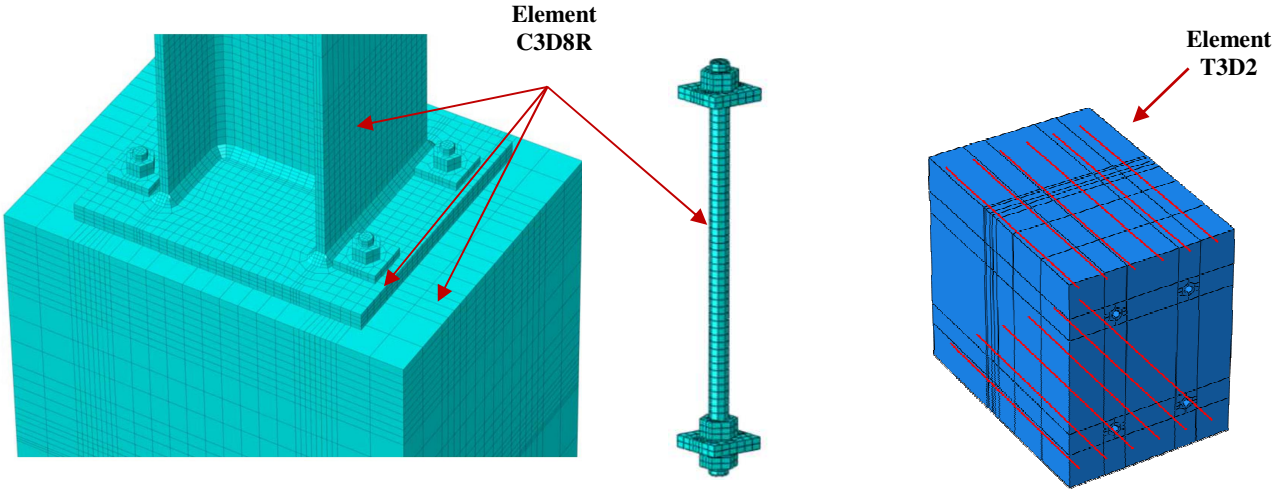

a) Connection, concrete block and column b) Anchor bolts c) Concrete bloc reinforcement

Fig. 1. *Type of finite elements*

The anchor bolts are modelled with nuts and washers and have a cross section area equal to $A = \pi d^2/4$ (d is the anchor bolt diameter). To produce reasonable and physically sound stress distributions at the interface between the anchor bolts and the concrete, a smaller mesh size was selected for the layer of concrete material in contact with the anchor bolts. In regions were buckling and/or severe bending were expected such as column flanges and base-plates, it was decided to assign three elements across the wall thickness of these thin elements and four for the 20 mm thickness base-plates. A sensitivity analysis confirmed that this meshing was adequate [17].

The material non-linearity was considered. The elasto-plastic behavior of steel components is described by the von-Mises yield criterion with strain hardening. The stress-strain curve introduced in the numerical models is multi-linear (see Fig. 2). The behavior is elastic up to the yield strength f_y. Next, the behavior is elastic-plastic up to ε_u. Material failure is simply characterized by an abrupt drop of the stress to 10 N/mm^2. This approach is appropriate to model the rupture of bolts in tension. The nominal characteristics of the materials are selected, and the steel grades of the column and the base plate are S355 and S275, respectively. The class of anchor bolts is 5.6. For concrete, the nominal properties of a C25/30 were considered. The material properties are summarized in Table 1.

Table 1 : *Material characteristics of the parametric study*

Column			Base Plate			Anchor bolts			Concrete	
$f_{y,c}$ (MPa)	$f_{u,c}$ (MPa)	$\varepsilon_{u,c}$ (%)	f_{yp} (MPa)	f_{up} (MPa)	$\varepsilon_{u,p}$ (%)	f_{yb} (MPa)	f_{ub} (MPa)	$\varepsilon_{u,b}$ (%)	f_{ck} (MPa)	$\varepsilon_{cu,1}$ (‰)
355	568	15	275	499	15	300	575	10	25	3,5

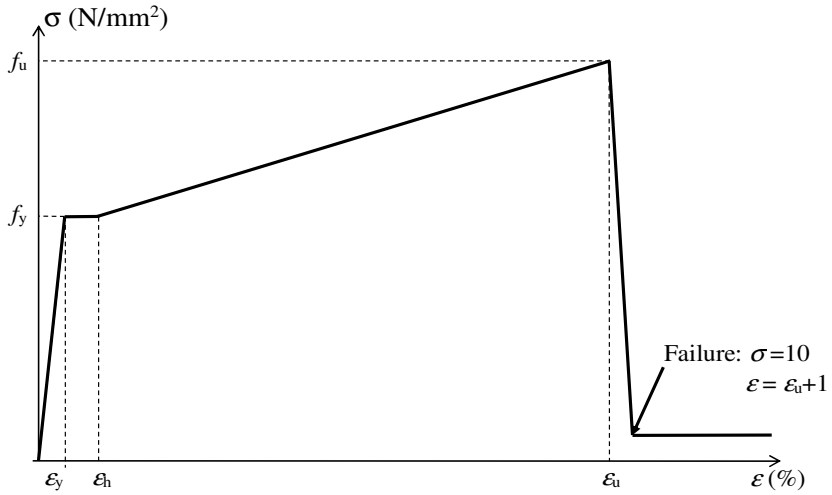

Fig. 2. *Stress-strain relationship for steel*

The compressive equivalent stress-strain curve proposed in EN 1992-1-1 was used to simulate the compressive behaviour of concrete. Concrete behaviour in tension and in compression are depicted in Fig. 3. Nominal values suggested in EN 1992-1-1 are used to define these curves. Concrete Damaged Plasticity model available in ABAQUS material library is used to simulate concrete behavior in compression and tension. Bond properties of the embedded anchor bolts were defined by a local bond-slip relationship taken from FIP Model Code 2010 [21] and presented in Fig. 4. The concrete material parameters used are presented in Table 2, further details can be found in [18].

Table 2 : *Concrete properties introduced in the FE model*

Concrete	f_{cm} (MPa)	ε_{c1} (‰)	f_{ctm} (MPa)	δ_{t1} (mm)
C25/30	25	2,1	2,6	0
Dilation angle (°)	Eccentricity	f_{b0}/f_{c0}	K	Viscosity parameter
36	0,1	1,16	0,667	0

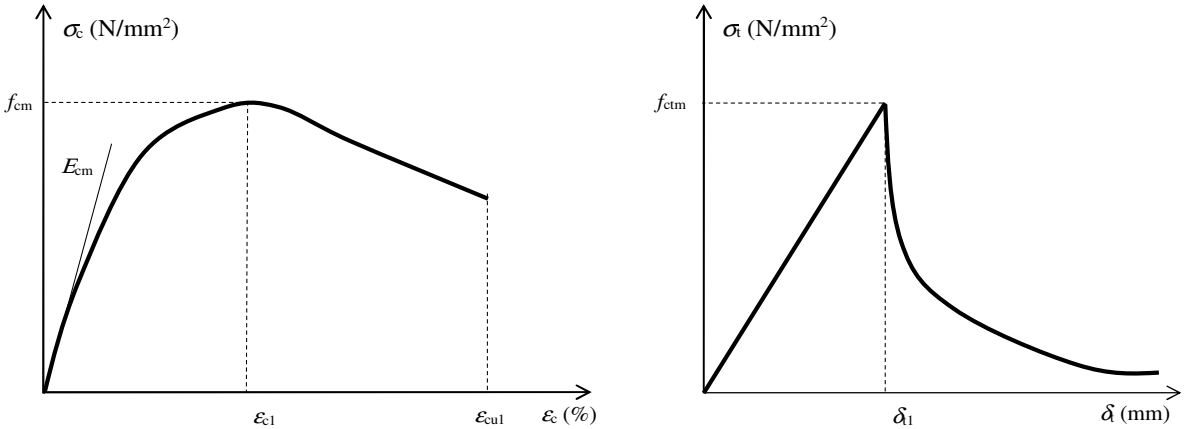

Fig. 3. *Stress-strain curve for concrete*

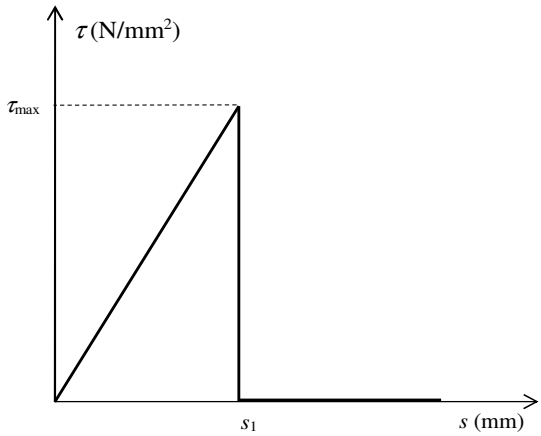

Fig. 4. *Bond stress-slip law from FIP Model Code 2010*

Kinematic constraints and contact interaction models adopted are listed below:

- "rigid body" constraint to create a rigid cross-section at the top of the column where the load is applied, and guarantee the uniformity of imposed displacement throughout the section. The reference point is located at the geometric centre of the column cross-section.
- "tie" constraint to connect the welds to the column and the base-plate.
- steel-steel and steel-concrete contacts considering friction coefficients equal to 0,3 and 0,5 for the former and latter, respectively. A surface-to-surface discretization method with finite sliding formulation is adopted. For normal behavior, the hard contact is selected allowing separation and preventing penetration of surfaces in contact,
- steel-concrete bonding interaction to model the contact between the lateral surface of the anchor bolts and the concrete block, a surface-to-surface contact type is selected with finite sliding formulation.
- "embedded region" constraint to create the contact interaction between the concrete and the steel reinforcement.

The loading was applied in two subsequent steps. The first step was defined to initiate contact interactions between the connection components. In the second step, the loading conditions were applied. Firstly, a constant value of the axial force was applied to the connection. Secondly, a displacement perpendicular to the centre line of the column steel profile was incrementally applied. As a consequence, the base-plate was subjected to an increasing bending moment with an arbitrary orientation until failure was reached. The failure was considered to be attained once:

- The von Mises strain reached the ultimate strain of the material ε_u in one steel component, the anchor bolts in the present study.
- The applied bending moment decreases due to column buckling.

During the loading, the axial force orientation coincide with the axis of the column. In addition great displacements and strain were considered in order to capture instability and necking.

2.3. *Geometry and loading conditions*

In this parametric study, six column base plate configurations have been investigated (P1 to P6) comprising base-plate welded either to HEA 200 (P1, P2, P5 and P6) or IPE 200 (P3 and P4) allowing to evaluate the effect of the column-shape on the connection's behaviour. The details of column base plate are given in Table 3 and Fig. 5. Fillet welds of 7 mm throat thickness connect the column profile to the base-plate. The base-plate is attached to a concrete block 460×360×725 mm of class C25/30 by means of four outer anchor bolts M16 or M20 class 5.6. The length of the column is equal to 500 mm to ensure proper stress flow but also to limit computational time and avoid column global buckling. Specimens were subjected to three different loading cases: pure bending moment about the strong axis, pure bending moment about the weak axis and biaxial bending moment with an orientation of the bending moment axis equal to 45°. The loading is identified by the letter M followed by a number specifying the inclination of the applied bending moment axis, *M0* for in-plane bending moment, *M90* for out-of-plane bending moment and *M45* for biaxial bending moment with an angle of 45°.

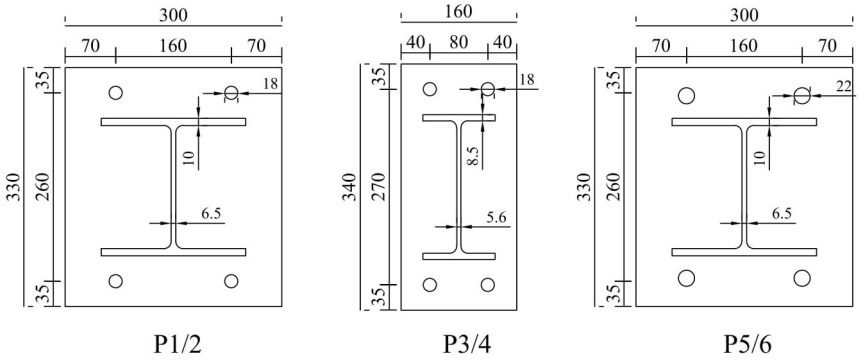

Fig. 5. *Geometry of specimens*

Specimens P1 and P2 are similar to connections tested by the authors [18] under in-plane, out-of-plane and biaxial bending moments. These connections are designed to investigate the influence of the base-plate thickness on the connection behaviour. The column, an HEA 200 typically used in practice, is connected to a base-plate of either 10 or 20 mm thickness, corresponding to specimen P1 and P2, respectively. Specimens P3 and P4 are composed of an IPE200 and the base plate thickness is varying. Specimens P5 and P6 are similar to specimens P1 and P2 with the exception of the anchor bolts

that are M20 instead of M16 for the latter. The objective was to analyse the effect of anchor bolt diameter.

Table 3 : *Geometries of the parametric study*

Configuration	Column steel profile	Base plate thickness t_p (mm)	Anchor bolt diameter (mm)
P1	HEA 200	10	16
P2	HEA 200	20	16
P3	IPE 200	10	16
P4	IPE 200	20	16
P5	HEA 200	10	20
P6	HEA 200	20	20

To evaluate the influence of a compressive/tensile axial force on the bending moment resistance and the failure modes of the connections, specimens are subjected to a combination of an axial force and uniaxial (in-plane/out-of-plane) or biaxial bending moments. To obtain the *M-N* ultimate interaction curves, specimens are firstly loaded by an axial force equal to a percentage of $N_{j,c,u}$ or $N_{j,t,u}$ which corresponds to the resistances obtained numerically in pure compression and tension, respectively. Next, they are loaded by a bending moment in one or two directions until failure. Table 4 summarizes the studied loading cases for specimens P1, P2, P3, P4, P5 and P6.

Table 4 : *Loading cases of the parametric study*

Axial force	Bending moment*	Axial force	Bending moment*
$N_{j,c,u}$	0	$N_{j,t,u}$	0
0	M0/M90/M45	-	-
$0,1\times N_{j,c,u}$		$0,1\times N_{j,t,u}$	
$0,2\times N_{j,c,u}$		$0,2\times N_{j,t,u}$	
$0,3\times N_{j,c,u}$		$0,3\times N_{j,t,u}$	
$0,4\times N_{j,c,u}$		$0,4\times N_{j,t,u}$	
$0,5\times N_{j,c,u}$	M0/M90/M45	$0,5\times N_{j,t,u}$	M0/M90/M45
$0,6\times N_{j,c,u}$		$0,6\times N_{j,t,u}$	
$0,7\times N_{j,c,u}$		$0,7\times N_{j,t,u}$	
$0,8\times N_{j,c,u}$		$0,8\times N_{j,t,u}$	
$0,9\times N_{j,c,u}$		$0,9\times N_{j,t,u}$	

*M0: in-plane bending moment; M90: out-of-plane bending moment; M45: biaxial bending moment.

2.4. *Failure modes/influence of the loading conditions*

Initial rotational stiffness, ultimate bending moments and failure modes of specimens P1 to P6 obtained for in-plane, out-of-plane and biaxial bending moments are summarized in the Appendix.

Two main failure modes are observed:

- Local buckling of the column flanges (see Fig. 6-a and Fig. 8-a for in-plane and out-of-plane bending moments, respectively) after substantial yielding,
- Failure of the anchor bolts in tension with or without base plate yielding (see Fig. 6-b/c and Fig. 8-b/c for in-plane and out-of-plane bending moments, respectively). For thicker base-plates, where yielding of the base plate does not develop in the tensile area, the compression area is located at the outer edge of the base plate (see Fig. 6-c and Fig. 8-c). For thinner base-plates, the compressive area develops between the outer edge of the plate and the column (see Fig. 6-b and Fig. 8-b) and the base-plate yields in the tensile area.

The M-N interaction curve obtained for in-plane bending moment is quite classical and has a multi-linear shape (see Fig. 6-d). For out-of-plane bending moment, the M-N interaction curve is clearly parabolic (see Fig. 8-d).

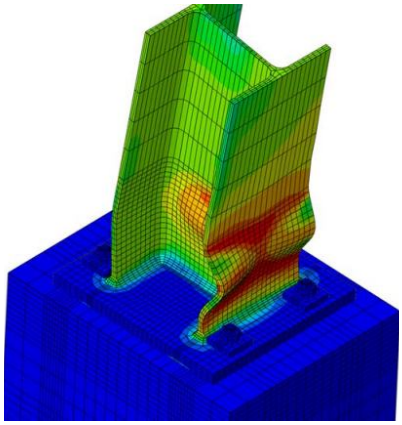

a) column local buckling

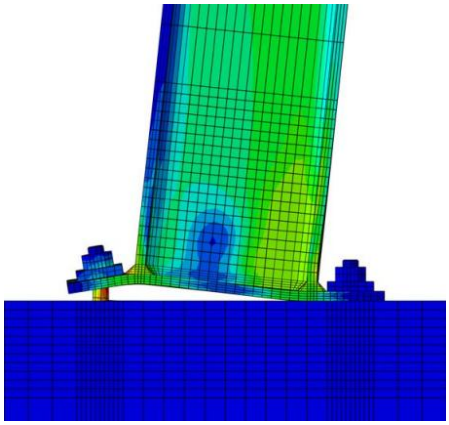

b) Anchor bolt failure with base-plate yielding

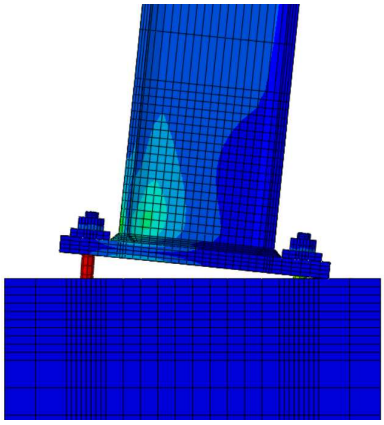

c) Anchor bolt failure without base-plate yielding

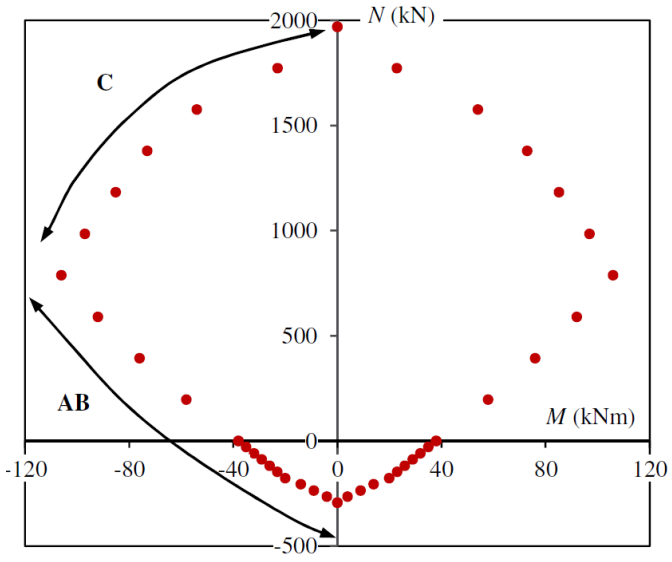

d) Interaction M-N curves for in-plane bending moment of specimen P1

Fig. 6. *Failure modes under in-plane bending moment*

The failure modes are strongly influenced by the loading. Under tensile force, all specimens considered in the present study failed by anchor bolt rupture in tension, regardless of the orientation of the bending moment axis. For values of the axial force up to $0{,}5N_{j,t,u}$, the anchor bolts in the tensile zone fail as a result of the combined action of local bending moment and tensile force. Above this value, the tensile force is dominant and nearly equally distributed among the anchor bolts. For this range of values of the applied tensile force, the elastic stage is very short and the post-limit strength is quickly reached. This can be verified from the comparison of the moment-rotation curves drawn for each specimens for different levels of tensile/compressive axial force (see Fig. 7). The in-plane rotation corresponds to the difference between the vertical displacements of the column flanges divided by the column depth. The displacements are measured at the intersection between the web and the flange centrelines. Under compressive force, the connection behavior is stiffer than that of a connection subjected to a tensile force, the compressed area being stiffer than the tensile zone. By increasing this area, the stiffness of the connection is increased.

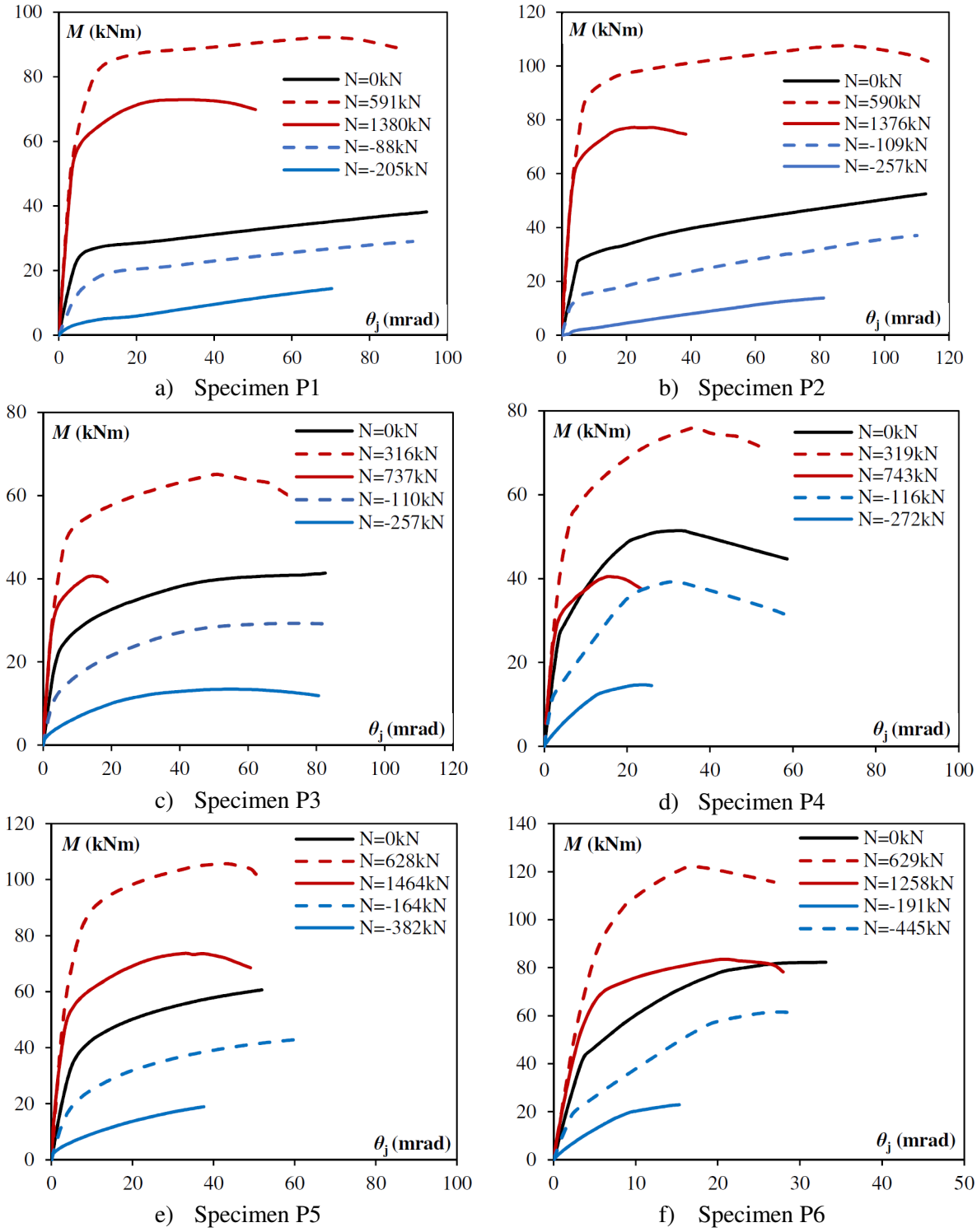

Fig. 7. *In-plane moment-rotation curves*

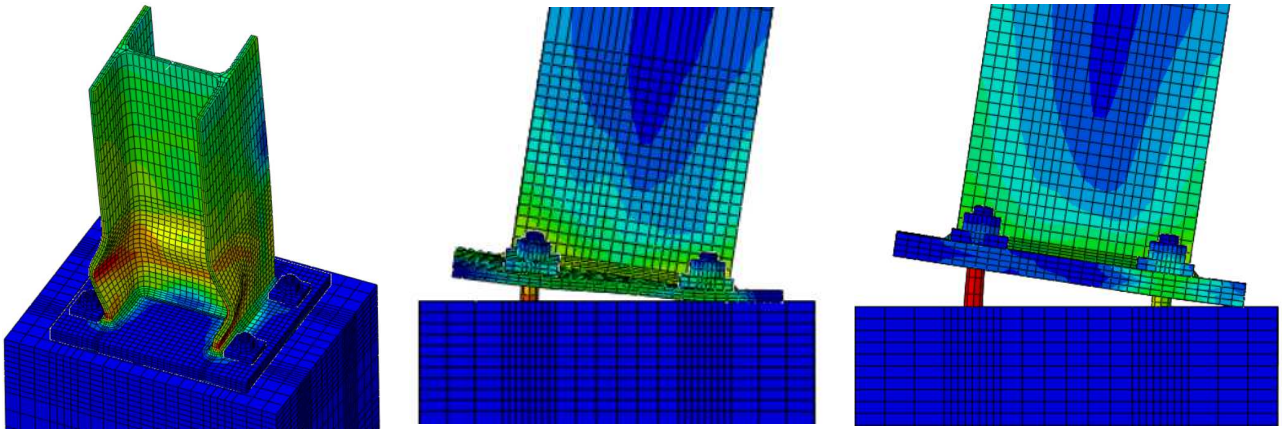

a) column flange buckling

b) Anchor bolt failure with base plate yielding

c) Anchor bolt failure without base plate yielding

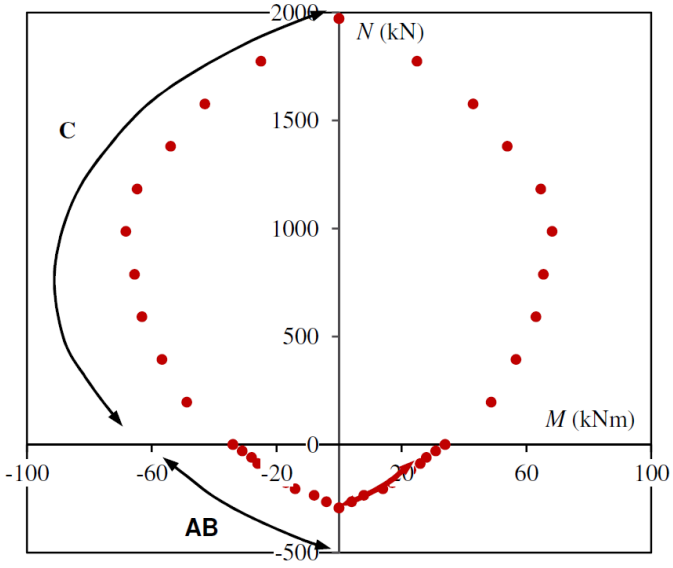

d) Interaction M-N curves for out-of-plane bending moment of specimen P1

Fig. 8. *Failure modes under out-of-plane bending moment*

The axial force also influence the ultimate bending moment $M_{j,u}$ and the initial rotational stiffness $S_{j,ini}$. From the Appendix, it can be observed that the ultimate bending moment and initial rotational stiffness decreases with increasing value of the tensile force regardless of the orientation of the bending moment axis. An increase of the tensile force produces a gradual decrease of the compressive area up to the point where the entire effective area of the base plate is working under tension. The compressive area being more rigid than the tensile area, the decrease of its area results in a decrease of the stiffness. Moreover, failure being caused by anchor bolt rupture in tension in presence of a pure bending moment, the application of a tensile force accelerate this phenomena.

In presence of a compressive force, the bending resistances and the initial rotational stiffness are increased for values of axial force up to $0{,}5N_{j,c,u}$. For M0 and M45 series, the tensile area which is at the

origin of the connection failure, is more flexible than the compressive area Therefore, the application of a compressive force to the connection unload this area. For M90 series, even if the failure is due to the local buckling of the column, the anchor bolts are subjected to high tensile forces. Then, the comments made above are also valid for this case. However, for values of the axial compressive force above $0{,}5N_{j,c,u,,}$ the resistance decreases as the failure is exclusively due to local buckling of the column.

Interaction curves of in-plane and out-of-plane bending moments, M_{ip}-M_{op}, are depicted in Fig. 9 and Fig. 10 for different compressive/tensile forces. The dots correspond to numerical results obtained for M0, M45 and M90. In addition, elliptical curves are drawn based on M0 and M90 results." In presence of a tensile force, the points of the numerical analysis fit quite well with an elliptical curve. However, for specimens P1 and P5 and values of the tensile force close to the tensile resistance, this elliptical curve is unsafe. It seems that a linear approximation is more suitable. For specimens P3 and P4, the elliptical curve is far from what is obtained numerically regardless of the value of the tensile force. In presence of a compressive force, the elliptical curve is generally conservative except for specimen P2 under high compressive force.

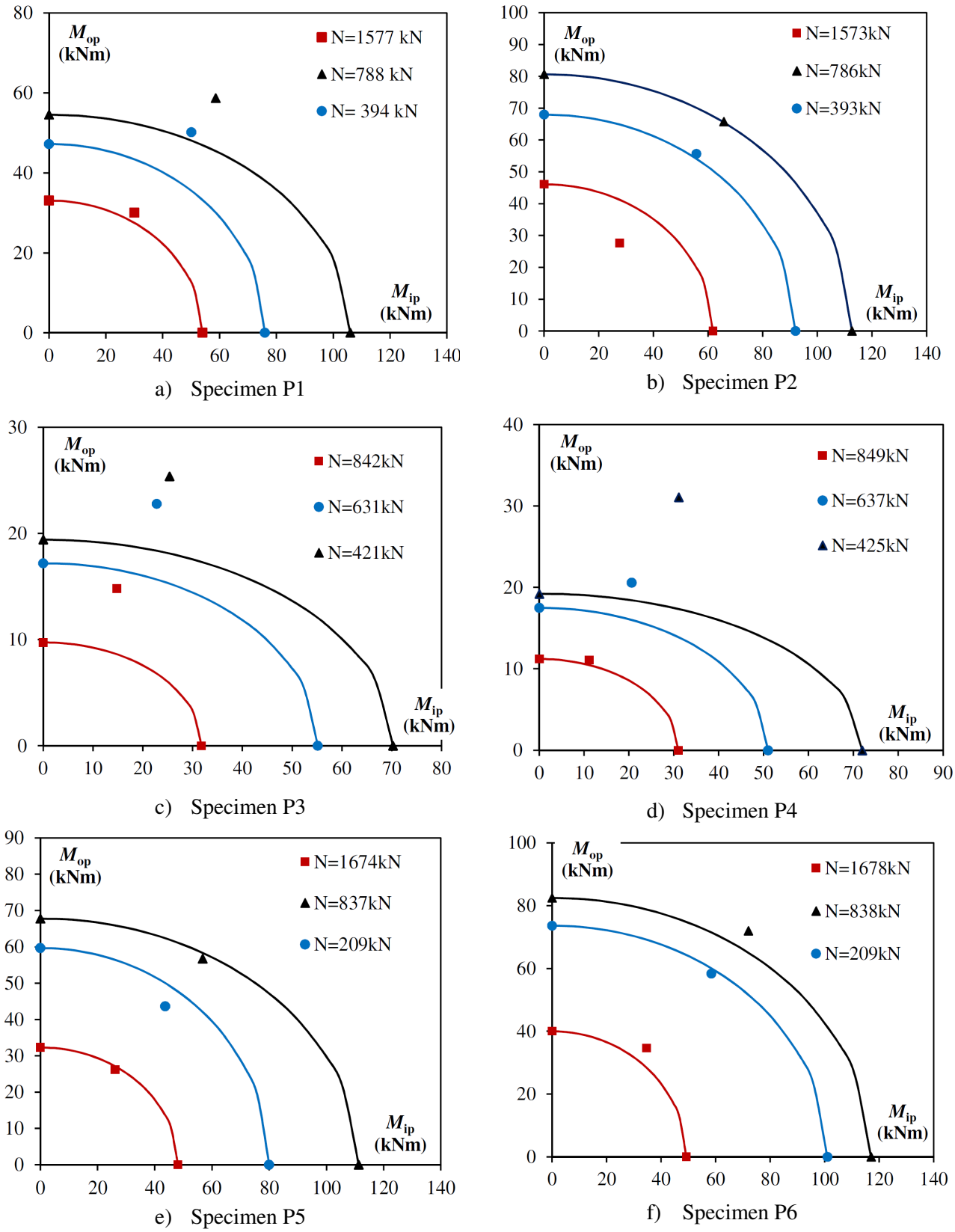

Fig. 9. Interaction curves M_{ip}-M_{op} under compressive force

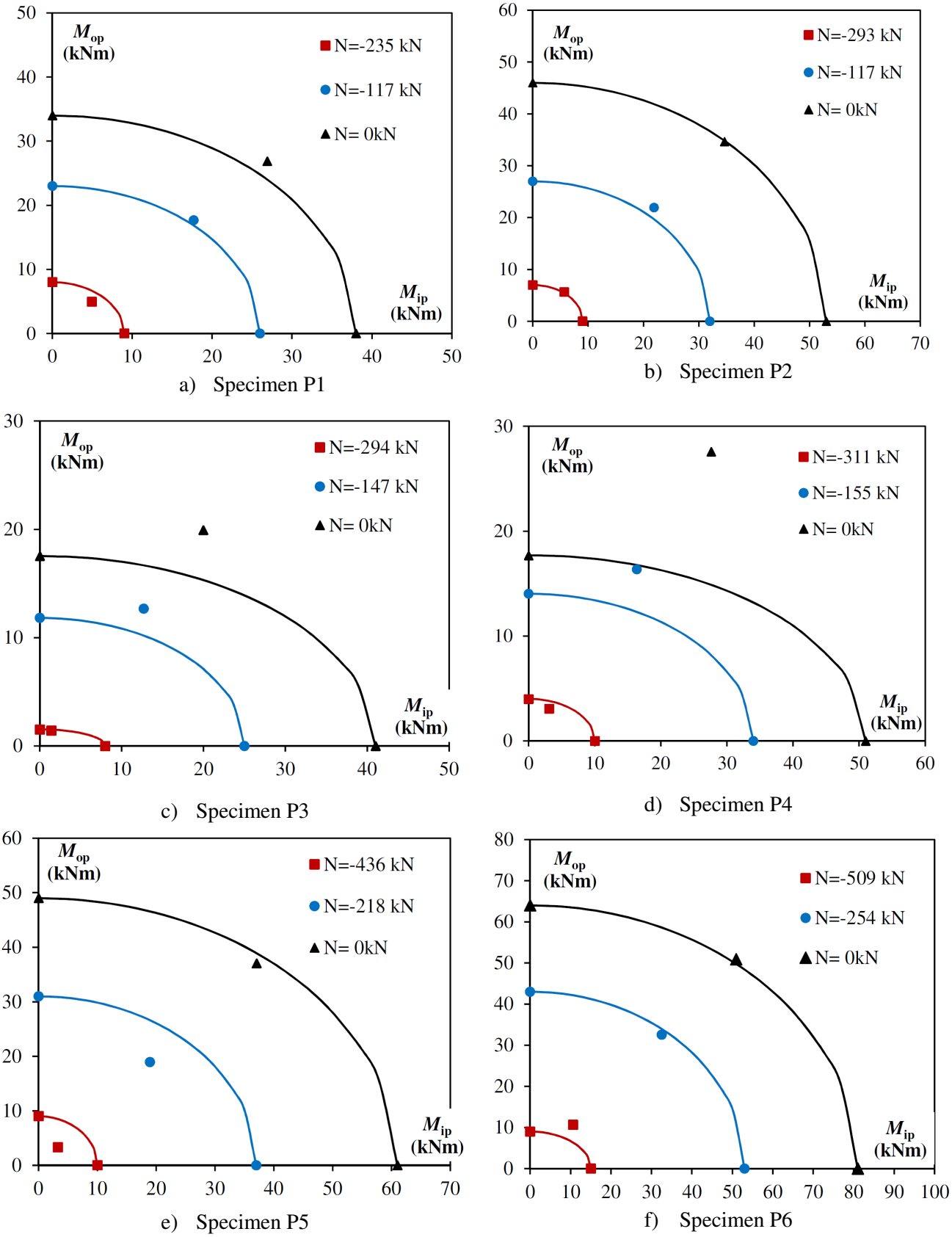

Fig. 10. Interaction curves M_{ip}-M_{op} under tensile force

2.5. *Influence of geometric parameters*

2.5.1. Base plate thickness

The influence of the base plate thickness is analyzed below in terms of failure mode, resistance and initial rotational stiffness. From the Appendix, it can be concluded that the base-plate thickness has no particular influence on the type of failure mode. Under combined bending moment and tensile force, anchor bolts govern failure of the connection regardless of the base-plate thickness. On the other hand, for connections subjected to combined compressive axial force and bending moment, two different failure modes can be observed: rupture of the anchor bolts in tension or local buckling of the column steel profile. The bending resistance increases with increasing values of the base-plate thickness. Increasing the base plate thickness leads to an increase of the lever arm z which corresponds to the distance between the center of compression and the center of tension. This increase limits also prying effects.

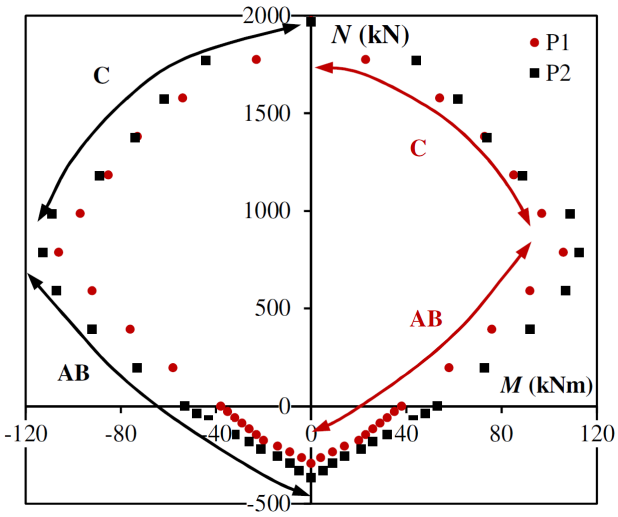

a) P1 and P2 under in-plane bending, M0

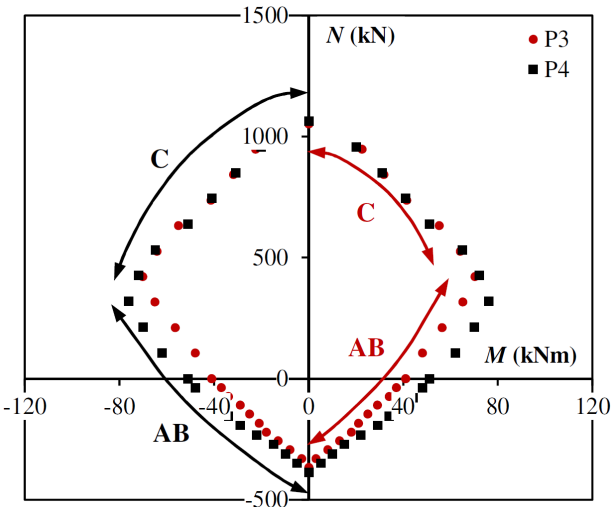

b) P3 and P4 under in-plane bending, M0

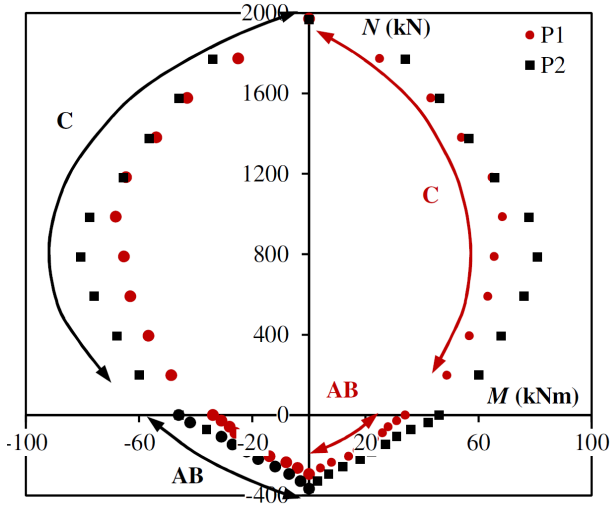

c) P1 and P2 under out-of-plane bending, M90

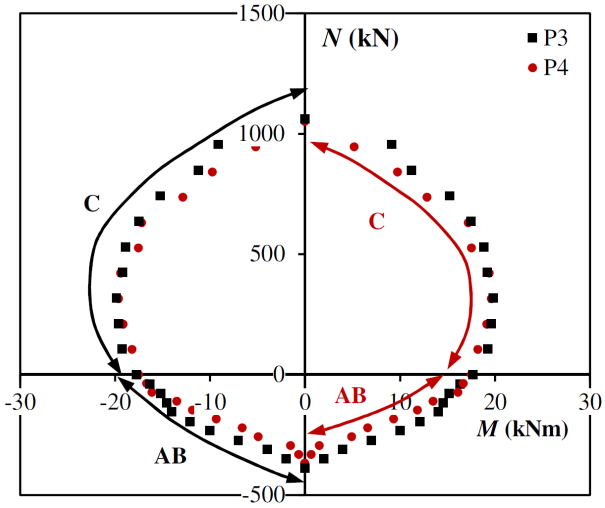

d) P3 and P4 under out-of-plane bending, M90

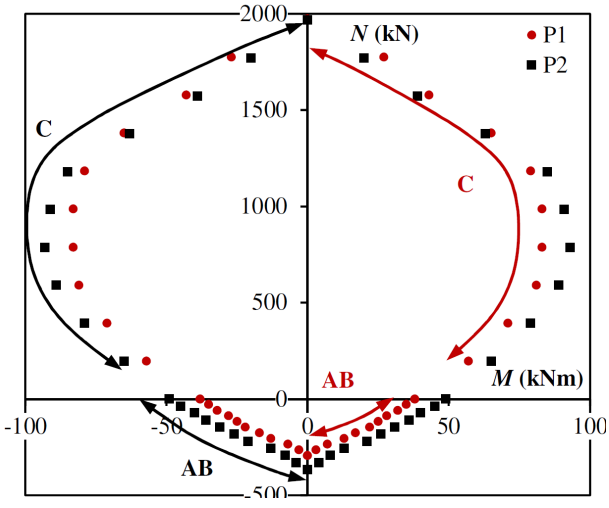

e) P1 and P2 under bi-axial bending, M45

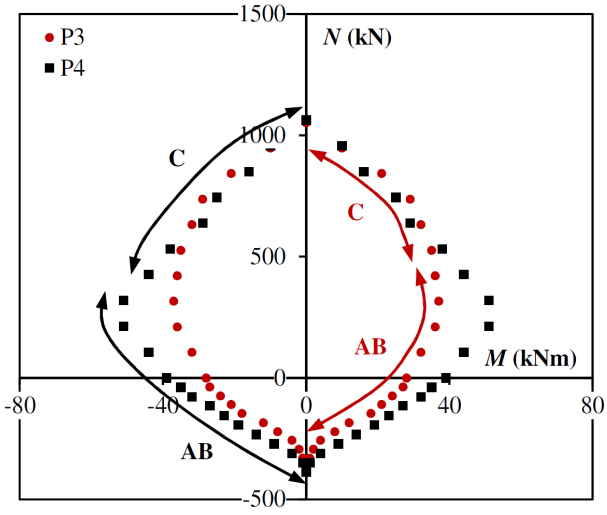

f) P3 and P4 under bi-axial bending, M45

Fig. 11. *M-N interaction curves: Influence of the base-plate thickness*

The increase of the base-plate thickness also affects the initial rotational stiffness of the connection. The initial rotational stiffness is larger for thicker base plates as a result of greater lever arm z and lower deformation of the base-plate in the tensile area. To get a better insight into the gain of resistance for the 20 mm base plate configuration, the *M-N* interaction curves are depicted in Fig. 11 for connections P1 to P4.

As observed, the gain in resistance is more or less evident, depending on the configuration of the connection and the applied loading conditions. For all cases, although less pronounced for out-of-plane bending, the gain in resistance is substantially higher when the failure mode is governed by anchor bolts rupture in tension. However, for values of the applied compressive force above $0{,}5N_{j,c,u}$, the curves overlap each other as a consequence of the local buckling of the column flanges. In these cases, the gain in resistance is insignificant. Under out-of-plane bending moment, the shape of the M-N curve is parabolic. For in-plane bending moment, it seems locally parabolic but in general, most of the segment of the curve is linear. The curve for biaxial bending moment are in between these two cases.

Contour plot of the contact pressure acting on the base-plate bottom surface (in contact with the concrete block) of connections P1 and P2 at failure are presented in Fig. 12 for in-plane bending moment. For an axial force equal to zero, the compression area is located close to the lower anchor bolt row for specimen P1 (see Fig. 12-a) and at the outer edge of the base plate for connection P2 (see Fig. 12-b). The lever arm are thus greater for thicker base-plate resulting in larger resistances and rotational stiffness. Under the maximal bending moment and the corresponding axial force, the compression area spread over the column flange for the two thickness's (see Fig. 12-c and d). The flange T-stub in compression is thus fully mobilized. Under pure compression, the contact area is greater for thicker base-plate (see Fig. 12-e and f). Stress concentration are also observed behind the welds that transfer the compression forces directly to the base-plate. The same conclusions can be drawn when comparing P3 and P4, as well as P5 and P6.

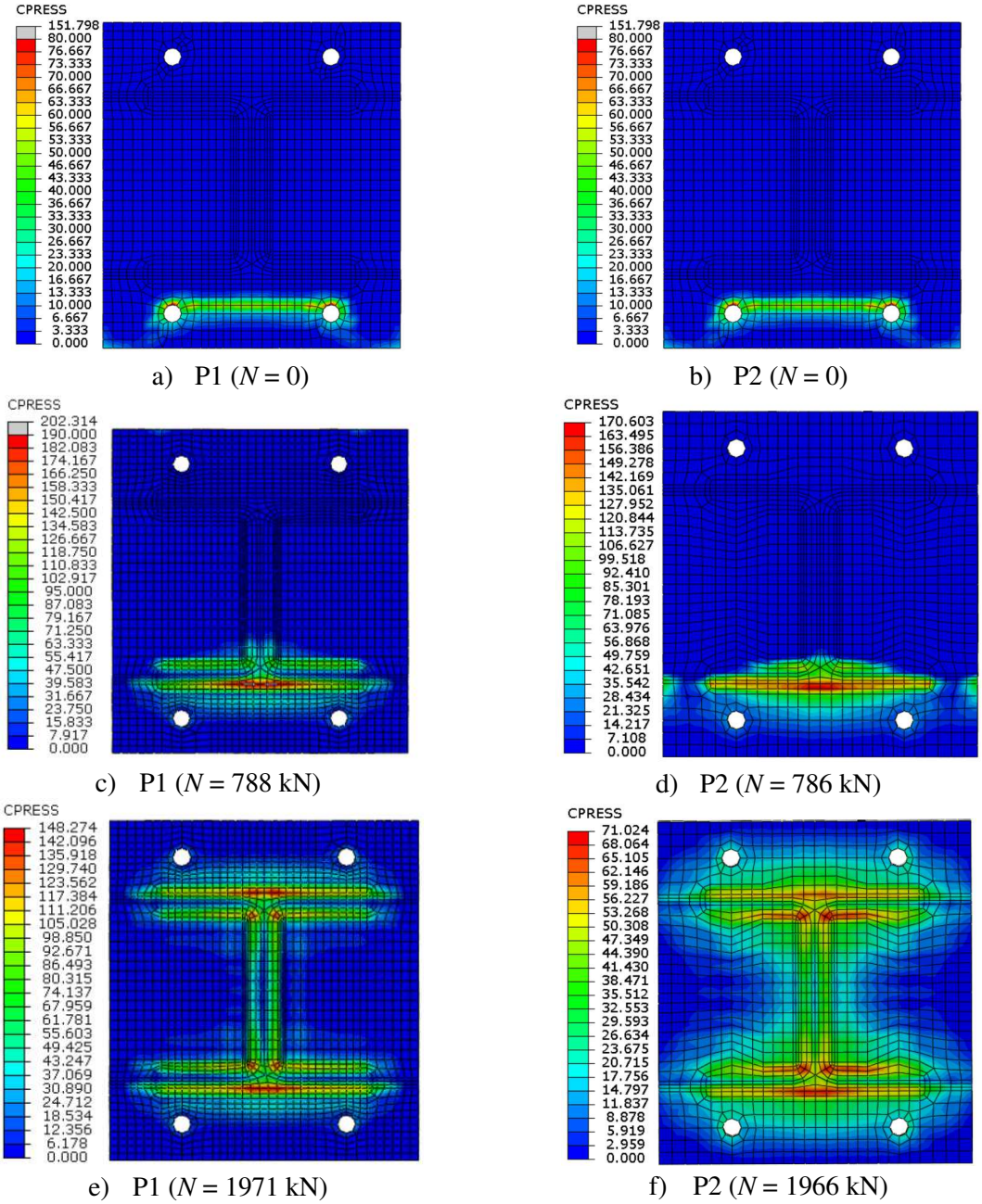

Fig. 12. *Contact pressures of P1 and P2 at failure for in-plane bending moment (in N/mm^2)*

Contour plot of the contact pressure acting on the base-plate bottom surface (in contact with the concrete block) of connections P1 and P2 at failure are presented in Fig. 13 for out-of-plane bending moment. In presence of pure out-of-plane bending moment, the contact pressure develop at the outer edge for thicker flange (see Fig. 13-b for connection P2) and at the corner of the column flange for the thinner ones (see Fig. 13-a for connection P1). This distinction induces a different lever arm that explains partially the modification of bending resistance and rotational stiffness. The contact area ex-

tends over nearly half the column flange when the maximum bending moment is applied to the connection (see Fig. 13-c and d).

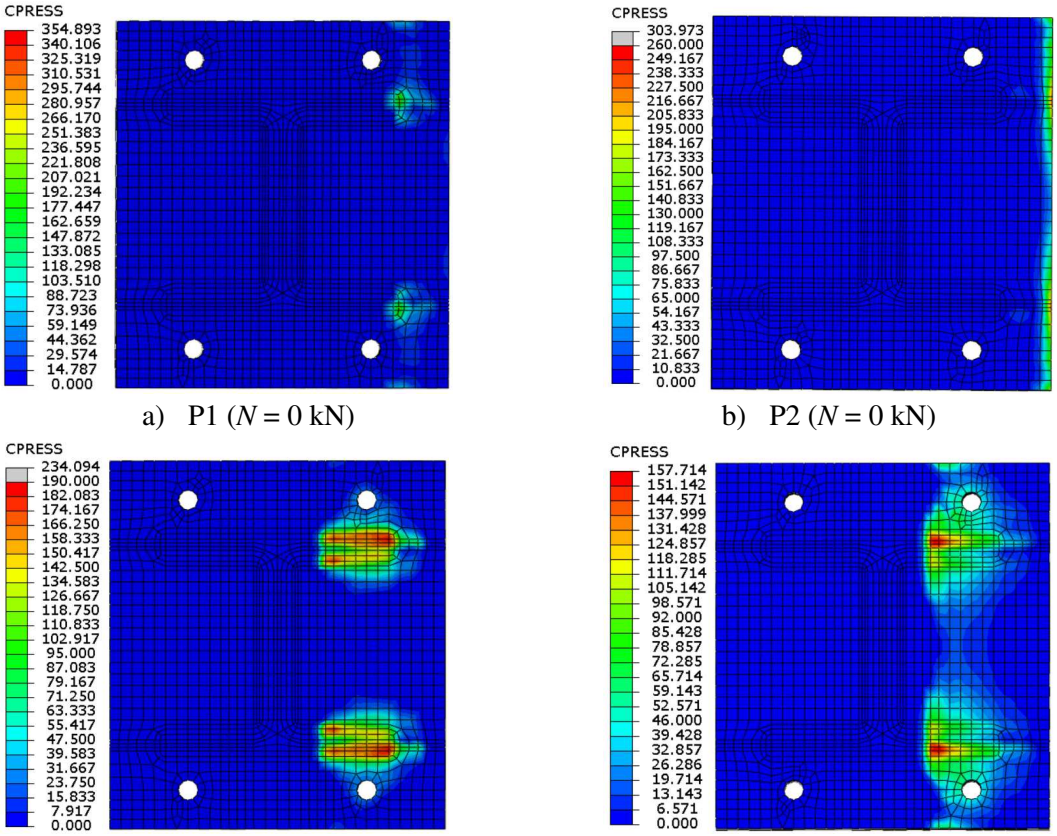

a) P1 (N = 0 kN) b) P2 (N = 0 kN)

c) P1 (N = 788 kN) d) P2 (N = 786kN)

Fig. 13. *Contact pressures of P1 and P2 at failure for out-of-plane bending moment (in N/mm^2)*

2.5.2. Column steel profile

Although HEA steel profiles are considered as the most suitable cross-sections for columns, IPE steel profiles are still widely used in practice. The influence of the steel column cross-section geometry (HEA 200 or IPE 200) on the connection response is discussed below. Interaction curves *M-N* depicted in Fig. 14, compare specimen P1 to specimen P3, and specimen P2 to specimen P4 under strong-axis, weak-axis and biaxial bending moments.

For a compression force larger than $0{,}5N_{j,c,u}$ and regardless of the orientation of the bending moment axis, the failure mode corresponds to column buckling. The bending resistance is thus strongly increased when an HEA 200 steel profile is used instead of an IPE 200.

Under combined in-plane bending moment and tensile force or low value of the compressive force, the bending resistance obtained with the two profiles are similar.

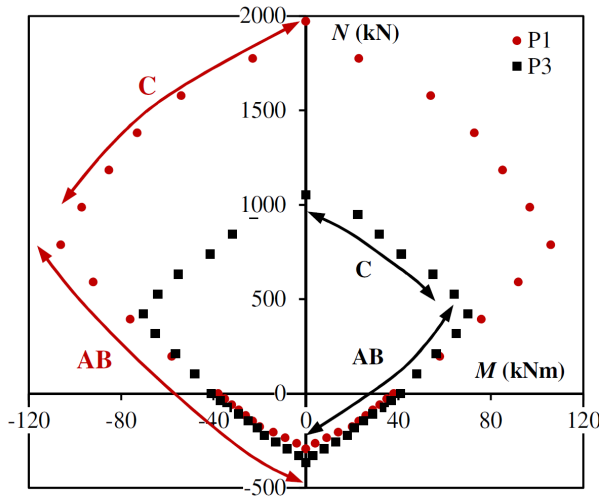

a) P1 and P3 under in-plane bending, M0

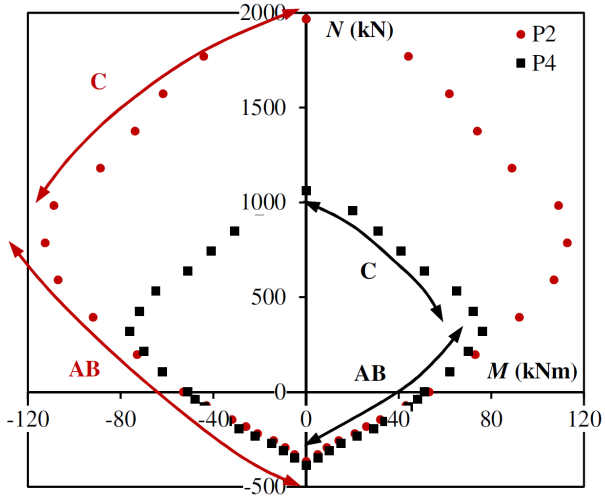

b) P2 and P4 under in-plane bending, M0

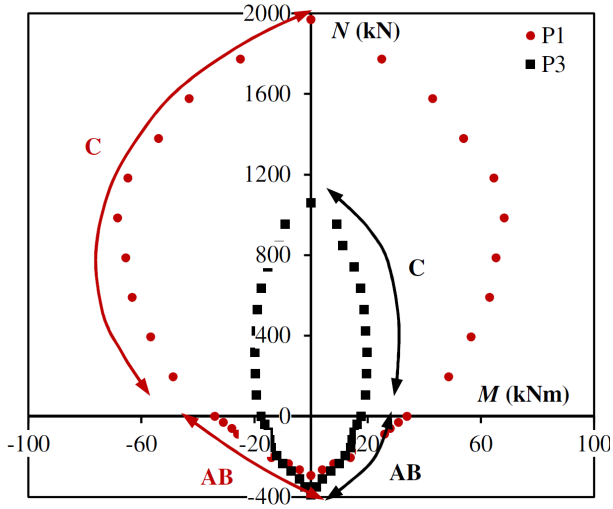

c) P1 and P3 under out-of-plane bending, M90

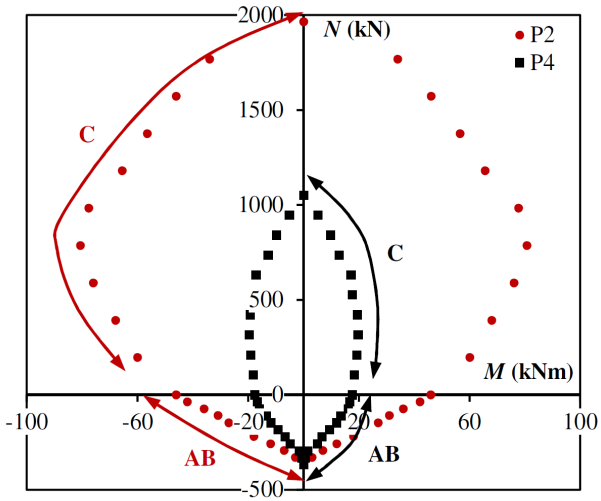

d) P2 and P4 under out-of-plane bending, M90

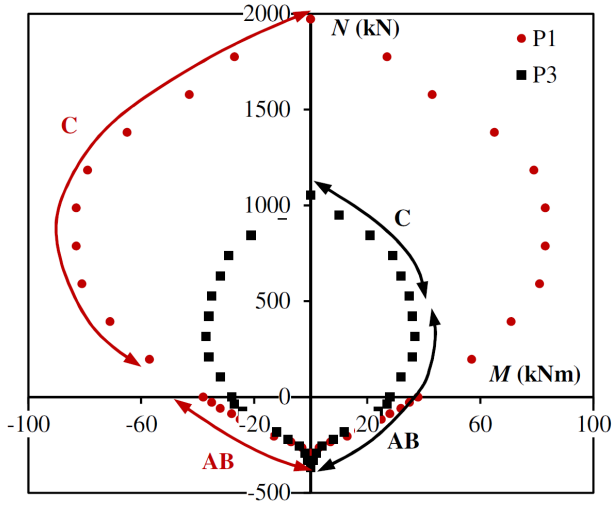

e) P1 and P3 under bi-axial bending, M45

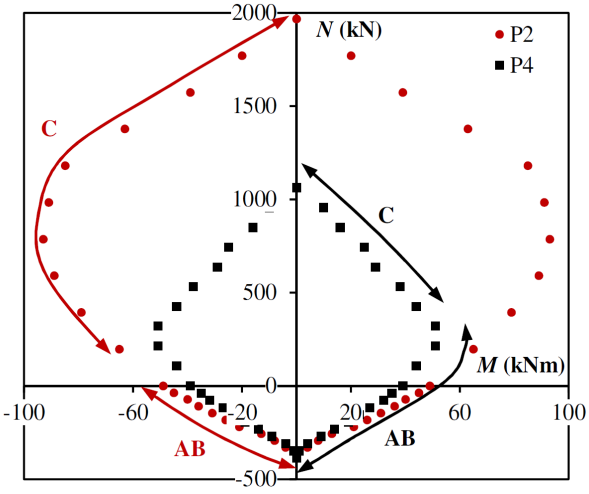

f) P2 and P4 under bi-axial bending, M45

Fig. 14. *M-N interaction curves: Influence of the column profile*

The lever arms with an HEA 200 or IPE 200 are quite close and only the base-plate width is different. The latter influence the local bending resistance of the base-plate in the tensile area. Furthermore, the decrease of the base-plate width reduces its flexibility and hence favour the development of prying effect (see Fig. 15-a and b). For out-of-plane bending moment, gain in resistance has been observed in presence of tensile or low value of the compressive force due to:

- the increase of the anchor bolt pitch that is beneficial in presence of dominant tensile force,
- the increase of the width of the column flange results in an increased lever arm in presence of dominant bending moment. The latter corresponds to the distance between the resultant forces in tension $F_{t,Rd}$ at the level of the tensioned anchor bolts, and the resultant forces in compression $F_{c,Rd}$ around the column flange corners that increases for the HEA 200 steel profile.

Similar results are obtained with biaxial bending moment. The contact pressure distributions are quite close for the two column shapes (see Fig. 15).

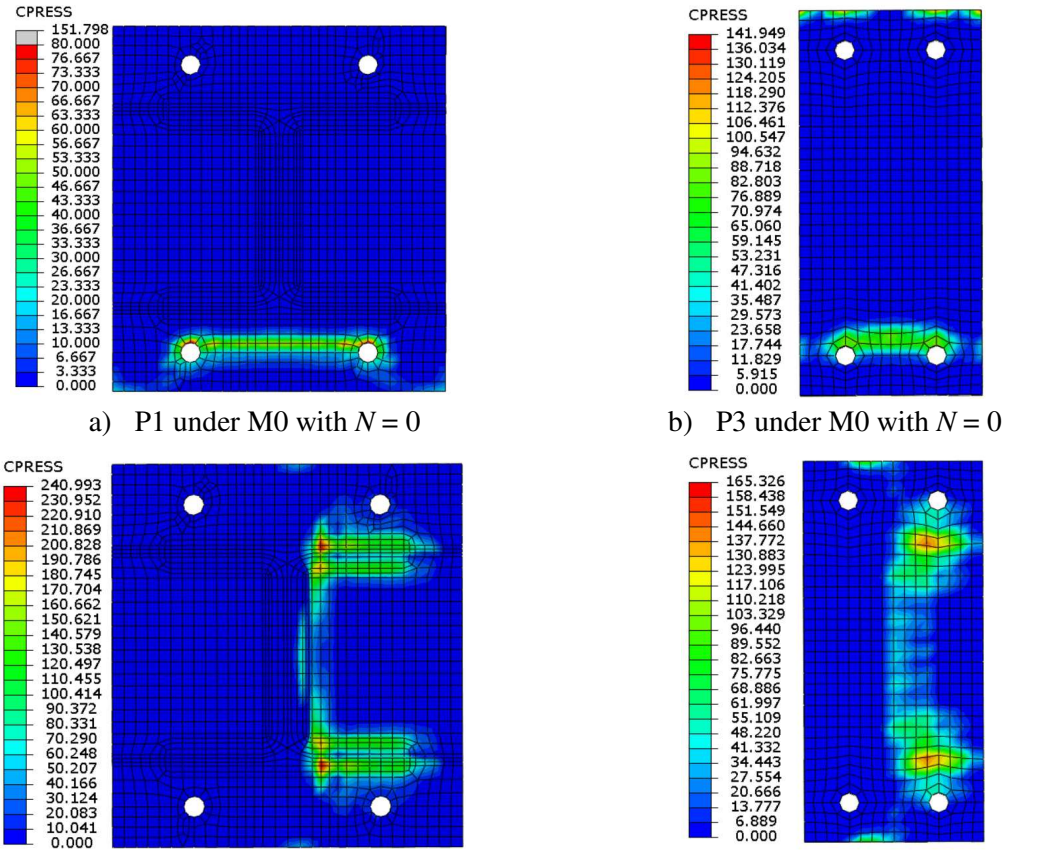

a) P1 under M0 with $N = 0$ b) P3 under M0 with $N = 0$

c) P1 under M90 with $N = 986$ kN d) P3 under M90 with $N = 316$ kN

Fig. 15. *Contact pressures for P1 and P3 at failure (in N/mm^2)*

2.5.3. Anchor bolt diameter

Anchor bolts strongly influence the behavior of column base plates. The impact of the anchor bolt diameter is investigated by comparing the response of connections P5 and P6 that use anchor bolts M20 against the response of connections P1 and P2 made with anchor bolts M16. The M-N interaction curves obtained for these four specimens are depicted in Fig. 17 for in-plane, out-of-plane and biaxial bending moments.

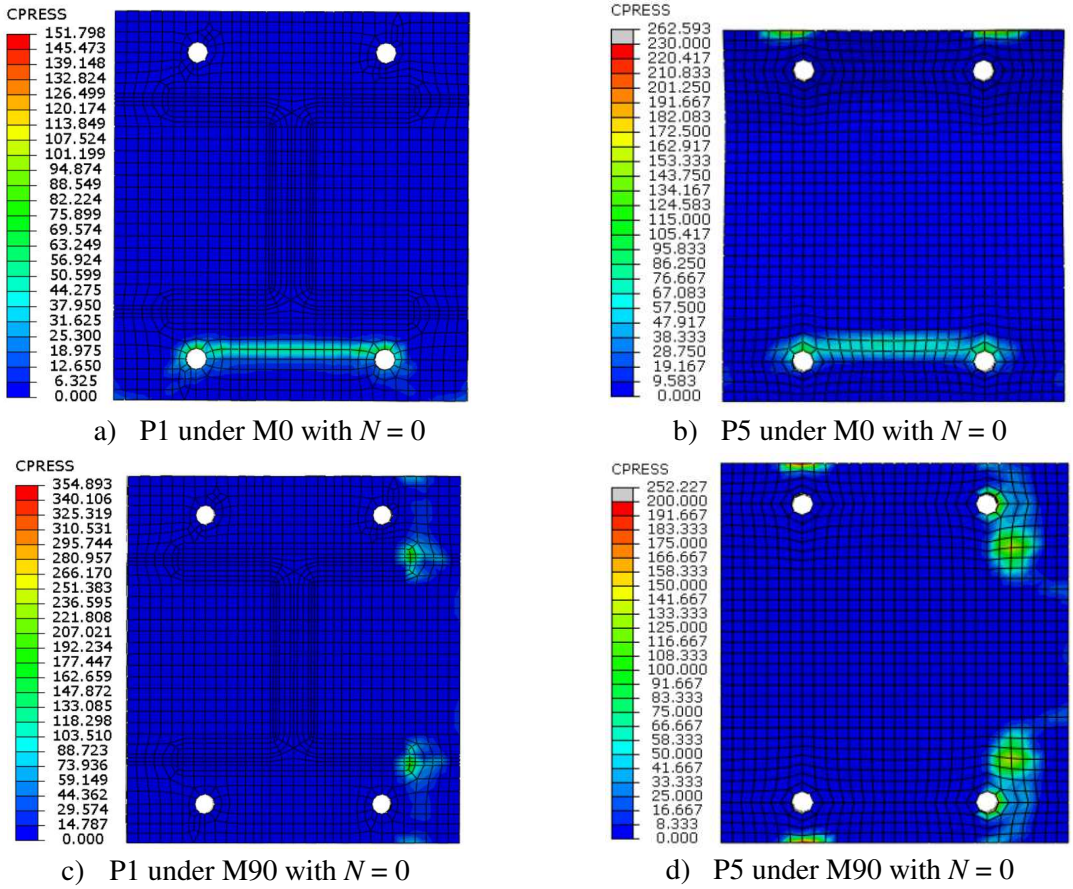

a) P1 under M0 with $N = 0$ b) P5 under M0 with $N = 0$

c) P1 under M90 with $N = 0$ d) P5 under M90 with $N = 0$

Fig. 16. *Contact pressures of P1 and P5 at failure (in N/mm^2)*

If failure is triggered by anchor bolt rupture in tension, the bending resistance of the connections is tremendously increased by an increase of the anchor bolt diameter regardless of the base-plate thickness.

Comparing the response of specimens P1 and P5 for in-plane bending moment, it can be seen that an increase of 50 % of the anchor bolts cross-section results in a 60% increase of the bending resistance. For the same loading case, an increase of about 70% is observed when comparing specimen P2 and specimen P6.

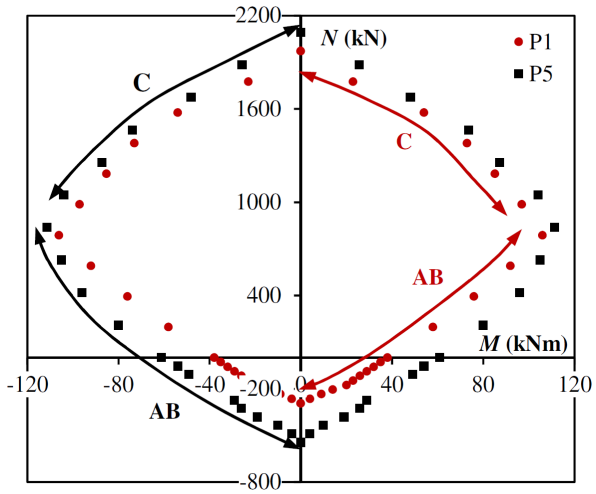

a) P1 and P5 under in plane bending, M0

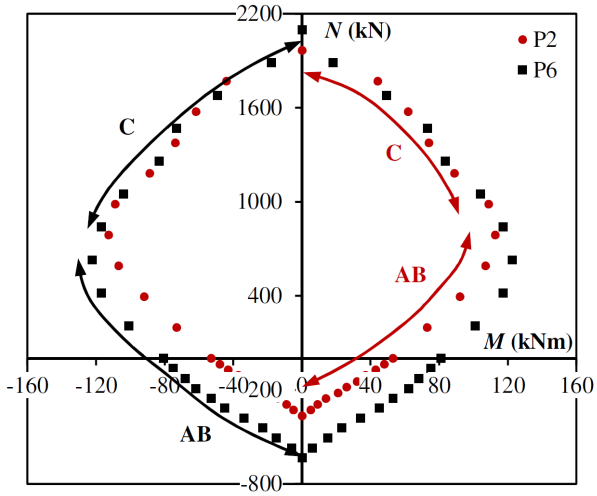

b) P2 and P6 under in plane bending, M0

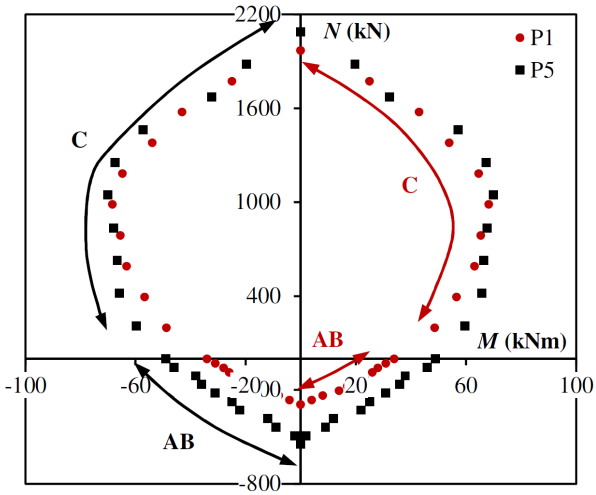

c) P1 and P5 under out-of-plane bending, M90

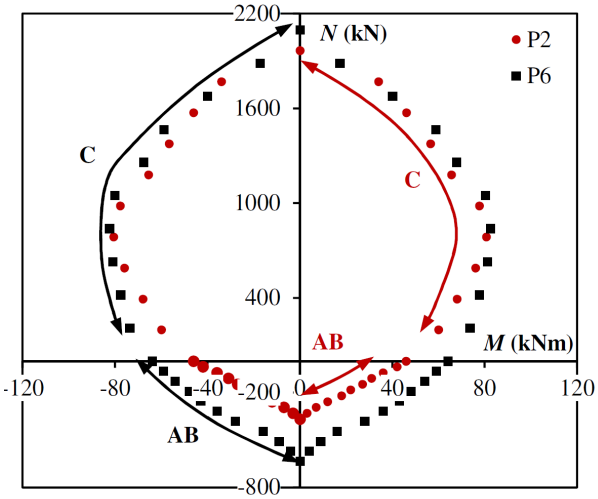

d) P2 and P6 under out-of-plane bending, M90

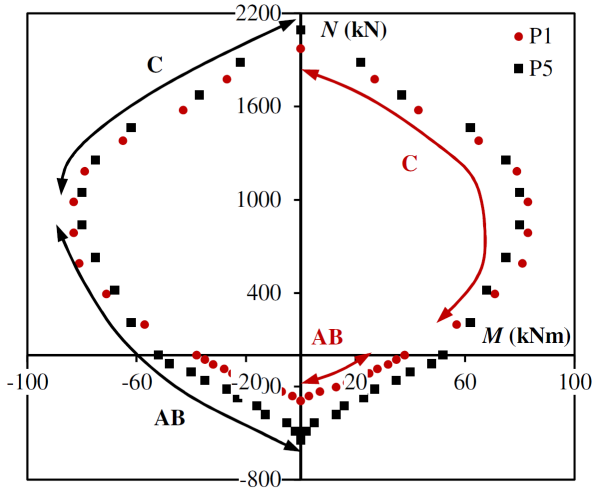

e) P1 and P5 under bi-axial bending, M45

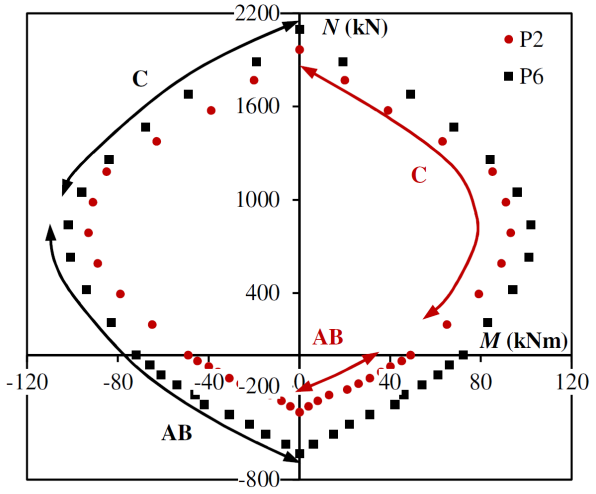

f) P2 and P6 under bi-axial bending, M45

Fig. 17. *M-N interaction curves: Influence of the anchor bolt diameter*

For out-of-plane and biaxial bending moments, the gains are also significant, up to 50% when comparing specimens P1 and P5 and 60% when comparing specimens P2 and P6. On the contrary, curves overlap when failure is due to column buckling particularly for compressive forces greater than $0{,}5N_{j,c,u}$. From the values presented in Appendix, a noticeable impact on the initial stiffness $S_{j,ini}$ is also observed. The anchor bolts being more rigid, the stiffness of the connection increases as well as prying effect, which becomes more evident for specimen P5 (see Fig. 16).

2.6. *Conclusions on the parametric study*

The parametric study highlighted the impact of base-plate thickness, anchor bolt diameter, bending moment orientation and axial load magnitude and character on the behaviour of column base plate. A particular attention was dedicated to initial rotational stiffness, ultimate bending resistance and failure mode. The main conclusions drawn from this study are given below:

- The failure mode strongly depends on the intensity of the axial force and on the orientation of the bending moment axis. In presence of tensile force, failure is caused by rupture of anchor bolts in tension regardless of the orientation of the bending moment axis. Increasing the applied tensile force decreases the bending moment resistance and the initial rotational stiffness regardless of the orientation of the bending moment axis. Increasing the compressive force up to half of the compressive resistance of the connection is advantageous in terms of resistance and initial stiffness for in-plane and biaxial bending moments (with an orientation of 45° of the bending moment axis). High compressive force generate local buckling/yielding in the column flanges, decreasing the resistance and initial stiffness of the connections.
- Increasing the base-plate thickness tends to improve the initial stiffness of the connections and its resistance if failure does not occur in the column.
- The use of an HEA steel profile instead of an IPE increases the lever arm in presence of dominant out-of-plane bending moment and consequently, increase the resistance.

- Increasing the anchor bolts diameter increases the bending resistance and the initial rotational stiffness of the connections particularly when failure corresponds to anchor bolt rupture in tension.
- The shape of the M-N curves is also affected by the orientation of the bending moment axis. For out-of-plane bending moment, a parabolic curve is clearly observed regardless of the studied configuration. For in-plane bending moment, the curve is more multi-linear. The interaction curve for biaxial bending moment with an angle of 45° is in between these two shapes.

3. ANALYTICAL MODEL

3.1. Introduction

In the present section, analytical models are proposed to evaluate the resistance of column base-plate under in-plane, out-of-plane and biaxial bending moments combined with axial force considering the principles of the component methods of Eurocode 3 and the following assumptions based on experimental and numerical observations:

- the resistance of the compressive area is estimated by adding the resistance provided by the flange to the resistance of the effective area around the web,
- the contact areas and lever arms of the compressive area are not fixed as in Eurocode 3 but depend on the base-plate thickness,
- for high compressive force, yielding can occur in the column. The resistance of the compressive area cannot exceed both the resistance of the concrete component and the strength of the column in compression, bounding the bearing strength f_{jd}.
- A plastic redistribution is considered regardless of the orientation of the bending moment axis.

3.2. General assumptions

The connections explored in this work consist in a rigid/semi-rigid extended base-plate welded to an I or H steel column. The extended base-plate is fastened to the concrete foundation by means of four outer anchor bolts. The design of the connection ensure that failure does not occur in the welds or the concrete block and that rupture of the connection is triggered by yielding of the base-plate and/or failure of the anchor bolts. Good contact conditions are assumed at the interface between the concrete block and the embedded length of the anchor bolts. The proposed models consider a plastic redistribution of the internal forces at failure. As abovementioned, the models are based on the basic assumptions of the Component Method from Eurocode 3. The components considered in the analytical model are the following:

- The components ensuring transfer of tensile force due to the bending moment are the base-plate in bending and the anchor bolts in tension;
- The components ensuring transfer of the compressive force due to bending moment are the concrete in compression, the base-plate in bending under bearing pressure exerted by the foundation and the column in compression.

The angle between the in-plane bending moment (see Fig. 18), M_{ip} and the resulting applied bending moment, M_u, is labelled α and thus it comes:

$$M_{ip} = M_u.\cos\alpha \quad (1)$$

$$M_{op} = M_u.\sin\alpha \quad (2)$$

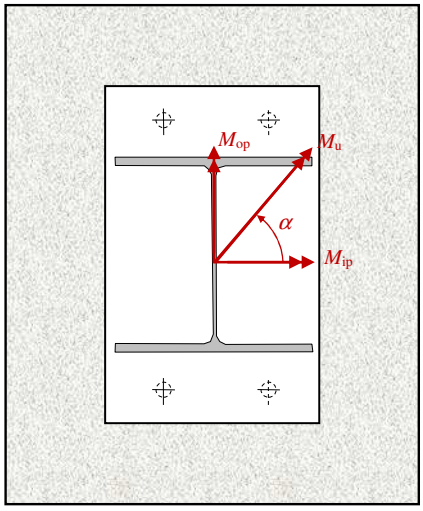

Fig. 18. *Bending moments orientation*

3.2.1 Components in tension

The ultimate resistance of the abovementioned components in tension $F_{T,u}$ is calculated according to Eurocode 3 part 1-8 [8] and corresponds to the lowest value of the resistance given by Modes 1, 2 and 3 (with prying effect) or Modes 1-2 and 3 (without prying effect). For Mode 1 and 1-2, the ultimate tensile strength f_u is used instead of the yield strength f_y. Additionally, for Mode 2, the base-plate yield strength f_y is replaced with $(f_y+2f_u)/3$ [16] to include strain hardening of this component before anchor bolt failure in tension.

3.2.2 Components in compression

According to the method suggested in Eurocode, the T-stub in compression is modelled considering the contribution of the base plate and the concrete foundation. From the parametric study, it can be observed that for high compressive force, the collapse of the connections tends to occur by yielding/buckling of the column. Thus, for the calculation of the resistance of the T-stub in compression, the minimum between the concrete foundation resistance and the column resistance is considered. The design resistance $F_{C,u,f}$ is obtained as follows:

$$F_{C,u,f} = \min\left(b_{eff,c} l_{eff,c} f_{jd,max};\ F_{c,u}\right) = b_{eff,c} l_{eff,c} f_{jd}^{*} \tag{3}$$

$$f_{jd}^{*} = f_{jd,max} \leq \frac{F_{c,u}}{b_{eff,c} l_{eff,c}} \tag{4}$$

with

$b_{eff,c}$, $l_{eff,c}$: column flange effective length and width in compression,

$f_{jd,max}$: design bearing strength of concrete calculated according to Eurocode 2 and 3,

$F_{c,u}$: maximum resistance of the column in compression.

The effective width and the effective length of the T-stub, $b_{eff,c}$ and $l_{eff,c}$ are obtained from Eurocode 3:

$$b_{eff,c} = \min\begin{cases} t_{fc} + 2c \\ \dfrac{h_p - h_c}{2} + t_{fc} + c \end{cases} \tag{5}$$

$$l_{eff,c} = \min\begin{cases} b_{fc} + 2c \\ b_p \end{cases} \tag{6}$$

with

t_{fc} : column flange thickness,

c : additional effective width,

h_p : height of the base-plate,

h_c : height of the column cross-section,

b_p : width of the base-plate,

b_{fc} : width of the column cross-section.

In the Component Method, the deformations of the base-plate should not exceed the elastic ones, assuming a uniform stress distribution under the base-plate and ensuring that the yield strength of the base plate is not exceeded. The effective bearing area is based on the effective width c that consider the elastic bending moment resistance per unit length of the base-plate. In the numerical analysis, yielding of the base plate in the compressive area was clearly observed and the plastic bending moment of the base plate was reached. In the proposed analytical models, the effective width c is obtained by equating the plastic bending moment resistance per unit length of the base plate to the bending moment per unit length acting on the base plate modelled by a cantilever beam of span c obtaining:

$$c = t_{\mathrm{p}} \sqrt{\frac{f_{\mathrm{y,p}}}{2 f_{\mathrm{jd,max}}}}$$

with

t_{p} : thickness of the base-plate,

$f_{\mathrm{y,p}}$: yield strength of the base-plate.

In this way, the value of the effective width c is increased and consequently the effective bearing area under the base plate, allowing to obtain values of the effective width that are less conservative and closer to those obtained by the numerical simulations. Numerical simulations also show that fillet welds allow to transfer compressive forces to the foundation. Thus, the width of the fillet welds is also added and the plastic bending moment is supposed to develop at the weld toe. Then, the additional effective width c is replaced by a modified effective width c^*:

$$c^* = t_{\mathrm{p}} \sqrt{\frac{f_{\mathrm{y,p}}}{2 f_{\mathrm{jd,max}}}} + \sqrt{2} a \tag{7}$$

with

a : weld throat thickness.

3.3. Bending resistance

3.3.1. In-plane bending resistance

Under in-plane bending moment, the model herein assumes different internal forces distributions according to the level of the applied loading and considering the additional resistance provided by the column web in compression. The model assumes that the anchor bolt tensile force is less than the tensile resistance when more than half of the web is under compression. In addition, the column failure is integrated directly in the model through the expression of the bearing strength. The four types of connection behaviour are identified in Fig. 19:

- dominant tensile force – a),
- dominant bending moment with critical tensile force – b) and c),
- dominant bending moment with critical compressive force – d),
- dominant compressive force – e).

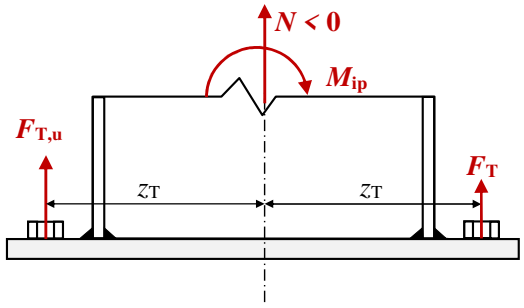

a) Dominant tensile force – behaviour type 1

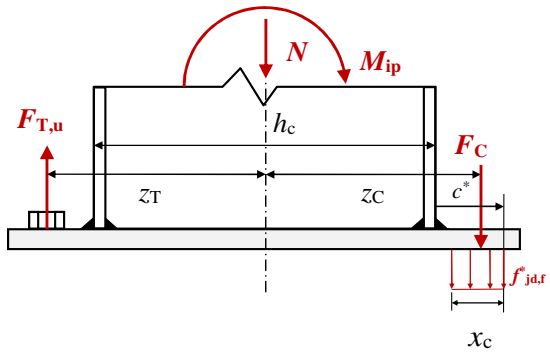

b) Dominant bending moment with critical tensile force and flange in compresion – behaviour type 2

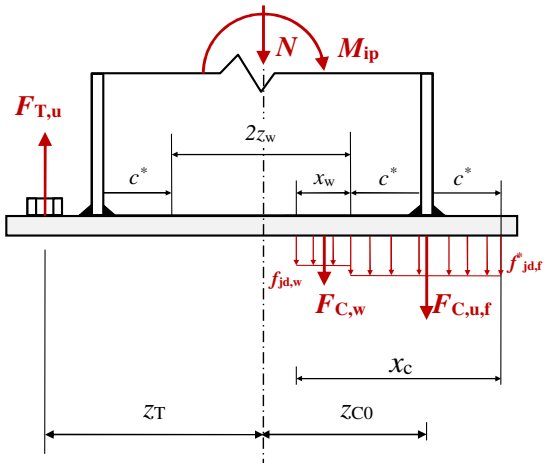

c) Dominant bending moment with critical tensile force and flange/web in compression– behaviour type 3

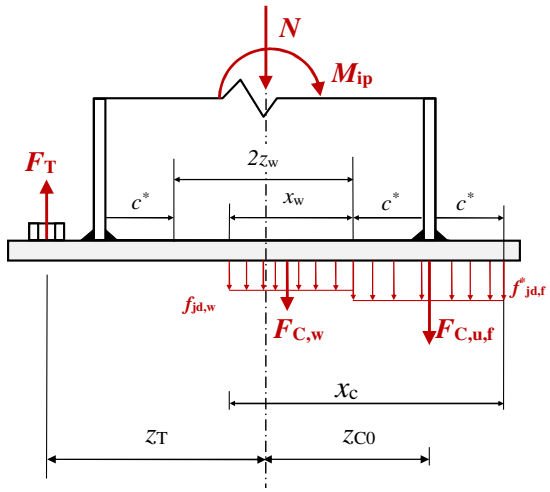

d) Dominant bending moment with critical compressive force –behaviour type 4

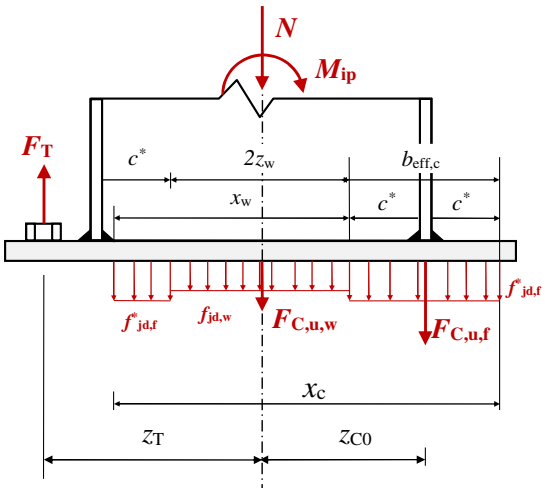

e) Dominant compressive force – behaviour type 5

Fig. 19. *Mechanisms considered for in-plane bending moment*

The validity domains of the aforementioned mechanisms are summarized below:

Table 5 : *Validity range of the mechanisms for in-plane bending moment*

Behaviour type	Loading	Range of validity
1	Dominant tensile force	$N_{T,u} \le N \le N_1$ $N_1 = -F_{T,u}$, $N_{T,u} = -2F_{T,u}$
2	Dominant bending moment with critical tensile force and flange in compression	$N_1 \le N \le N_2$ $N_2 = F_{C,u,f} - F_{T,u}$
3	Dominant bending moment with critical tensile force and flange/web in compression	$N_2 \le N \le N_3$ $N_3 = F_{C,u,f} + F_{C,u,w}/2 - F_{T,u}$
4	Dominant bending moment with critical compressive force	$N_3 \le N \le N_4$ $N_4 = F_{C,u,f} + F_{C,u,w}$
5	Dominant compressive force	$N_4 \le N \le N_{C,u}$ $N_{C,u} = 2F_{C,u,f} + F_{C,u,w}$

In presence of dominant tensile force (see Fig. 19-a), Eurocode 3 Part 1-8 is applied for the determination of the ultimate bending moment resistance $M_{ip,u}$. The internal forces system comprises two resultant forces $F_{T,u}$ and F_T acting on both sides at the anchor bolts axes. Then, the in plane bending resistance is given by:

$$M_{ip,u} = 2z_T F_{T,u} + z_T N \tag{8}$$

with

$F_{T,u}$: resistance of the T-stub in tension (see section 3.2.1),

N : axial force,

z_T : lever arm of the tensile area (distance between the line of action of the anchor bolts and the center of the column).

Under dominant bending moment and critical tensile force (see Fig. 19-b), the position of the neutral axis depends on the axial force and the resistance of the tensile area. The equilibrium of axial forces gives:

$$N = f_{jd,f}^{*} l_{eff,c} x_c - F_{T,u} \tag{9}$$

The bearing resistance is limited to the resistance in compression of the flange and column web evaluated according to Eurocode 3 part 1-8, $F_{c,fc,u}$, thus:

$$f_{jd,f}^{*} = \frac{F_{c,fc,u}}{b_{eff,c} l_{eff,c}} \le f_{jd,max} \tag{10}$$

$$F_{c,fc,u} = \frac{W_{pl,c} f_{y,c}}{h_c - t_{fc}} \tag{11}$$

with

$W_{pl,c}$: column cross-section plastic modulus,

$f_{y,c}$: column yield strength.

One obtain the position of the neutral axis x_c:

$$x_c = \frac{N + F_{T,u}}{l_{eff,c} f^*_{jd,f}} \leq t_{fc} + 2c^* \tag{12}$$

The in-plane bending resistance is thus:

$$M_{ip,u} = F_{T,u} \left(z_T + z_C \right) + z_C N \tag{13}$$

with

z_C : compressive lever arm (distance between the line of action of the resultant compressive force F_C and the centre of the column):

$$z_C = h_c / 2 + c^* - x_c / 2 \tag{14}$$

Behaviour type 3 (see Fig. 19-c) corresponds to the case in which the effective width of the column flange $b_{eff,c}$ is fully under compression ($x_c \geq t_{fc} + 2c^*$). As a result, $F_{C,u,f}$ and $F_{T,u}$ can develop. Also, part of the column web is contributing to the resistance of the connection. The force transmitted by the column web is denoted $F_{C,w}$. This system of internal forces is valid provided that the following criteria are respected:

$$x_c = b_{eff,c} + x_w \tag{15}$$

$$x_w \leq z_w \tag{16}$$

with

z_w : half of the total effective length of the web in compression, $l_{eff,w}$,

x_w : portion of the effective web in compression.

The equilibrium of axial forces gives:

$$N = F_{C,u,f} + f_{jd,w} b_{eff,w} x_w - F_{T,u} \quad (17)$$

with

$F_{C,u,f}$: resistance of the column flange T-stub in compression considering $f_{jd} = f_{jd,f}^*$,

$b_{eff,w}$: column web effective width :

$$b_{eff,w} = t_{wc} + 2c^*$$

$f_{jd,w}$: design bearing strength of the web:

$$f_{jd,w} = \frac{N_{C,u} - 2F_{C,u,f}}{2b_{eff,w} z_w} \le f_{jd,max}$$

Thus the length of the web in compression is:

$$x_w = \frac{N + F_{T,u} - F_{C,u,f}}{b_{eff,w} f_{jd,w}} \quad (18)$$

The in-plane bending moment resistance is given by:

$$M_{ip,u} = F_{T,u} z_T + F_{C,u,f} z_{C0} + x_w b_{eff,w} f_{jd,w} \left(z_w - x_w / 2 \right) \quad (19)$$

Behaviour type 4 (see Fig. 19-d) corresponds to the case in which the effective width of the column flange and more than half of the web effective length are fully under compression. This system of internal forces is valid provided that the following criteria are respected:

$$b_{eff,c} + z_w \le x_c \le b_{eff,c} + 2z_w \quad (20)$$

$$z_w \le x_w \le 2z_w \quad (21)$$

With more than half of the effective area of the base plate under compression, it has been observed numerically (see section 2.4) that failure does not occur in the tensile area and, as a result, it is proposed to reduce the tensile force F_T as follows:

$$F_T = F_{T,u} \frac{2z_w - x_w}{z_w} \le F_{T,u} \quad (22)$$

The tensile force transmitted by the anchor bolts is thus equal to zero when the left flange T-stub in compression is mobilized.

The equilibrium of the axial forces gives:

$$N = F_{\mathrm{C,u,f}} + f_{\mathrm{jd,w}} b_{\mathrm{eff,w}} x_{\mathrm{w}} - F_{\mathrm{T}} \tag{23}$$

The length of the web in compression is calculated from:

$$x_{\mathrm{w}} = \frac{N + 2F_{\mathrm{T,u}} - F_{\mathrm{C,u,f}}}{b_{\mathrm{eff,w}}\, f_{\mathrm{jd,w}} + F_{\mathrm{T,u}} / z_{\mathrm{w}}} \tag{24}$$

The in-plane bending moment resistance is given by:

$$M_{\mathrm{ip,u}} = F_{\mathrm{T}} z_{\mathrm{T}} + F_{\mathrm{C,u,f}} z_{\mathrm{C0}} + x_{\mathrm{w}} b_{\mathrm{eff,w}} f_{\mathrm{jd,w}} \left(z_{\mathrm{w}} - x_{\mathrm{w}} / 2 \right) \tag{25}$$

Behaviour type 5 (see Fig. 19-e)) corresponds to a dominant compressive force. The ultimate in-plane bending moment resistance is obtained as follows:

$$M_{\mathrm{ip,u}} = \left[b_{\mathrm{eff,c}} - (x_{\mathrm{w}} - 2z_{\mathrm{w}}) \right] l_{\mathrm{eff,c}} f^{*}_{\mathrm{jd,f}} \left[\frac{h_{\mathrm{c}}}{2} + c^{*} - \frac{(b_{\mathrm{eff,c}} - (x_{\mathrm{w}} - 2z_{\mathrm{w}}))}{2} \right] \tag{26}$$

with

$$x_{\mathrm{w}} = \frac{N - F_{\mathrm{C,u,f}} - F_{\mathrm{C,u,w}} + 2z_{\mathrm{w}} l_{\mathrm{eff,c}}\, f^{*}_{\mathrm{jd,f}}}{l_{\mathrm{eff,c}}\, f^{*}_{\mathrm{jd,f}}}$$

3.3.2. Out-of-plane bending resistance

A simplified model is proposed for the calculation of the resistance of column base plates subjected to combined axial force and out-of-plane bending moment. The final proposal is based on a parabolic interaction that was suggested by the parametric study (see section 2). A simple parabolic expression of the M-N interaction curve is firstly proposed for the force distribution shown in Fig. 20. It is assumed that the out-of-plate bending moment is balanced by an uniformly distributed force in the tensile and compressive areas along the effective length of the column flange $l_{\mathrm{eff,c}}$ (see Fig. 20). Concerning the compressive area, this hypothesis seems rational. For the tensile area, the lever arm can be underestimated or overestimated (depending on the position of the anchor bolts) and so the maximum bending moment. To evaluate the contribution of both compressive and tensile sides $f_{\mathrm{c,u}}$ and $f_{\mathrm{t,u}}$, the position of the neutral axis x_{c} must be determined.

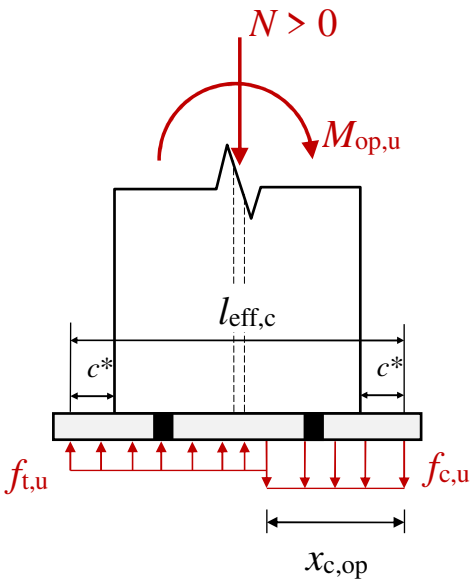

Fig. 20. *Simplified mechanism of internal forces for out-of-plane bending moment*

The uniformly distributed resistances along the column flange effective width $f_{t,u}$ and $f_{c,u}$ are calculated as follows:

$$f_{t,u} = \frac{N_{T,u}}{l_{eff,c}} \tag{27}$$

$$f_{c,u} = \frac{N_{C,u}}{l_{eff,c}} \tag{28}$$

with

$N_{T,u}$: tensile resistance of the connection,

$N_{C,u}$: compressive resistance of the connection.

The equilibrium of axial forces gives:

$$N = f_{c,u} x_{c,op} - f_{t,u} (l_{eff,c} - x_{c,op}) \tag{29}$$

Inserting (27) and (28) in (29), one obtain the position of the neutral axis $x_{c,op}$:

$$x_{c,op} = l_{eff,c} \frac{N + N_{T,u}}{N_{C,u} + N_{T,u}} \tag{30}$$

The ultimate bending moment resistance $M_{op,u}$ is obtained from:

$$M_{op,u} = M_{C,u} + M_{T,u} + N\left(\frac{l_{eff,c}}{2} - x_{c,op}\right) \tag{31}$$

with

$M_{C,u}$: bending moment about the neutral axis produced by the force acting in the compressive area:

$$M_{C,u} = f_{c,u} \frac{\left(x_{c,op}\right)^2}{2}$$

$M_{T,u}$: bending moment about the neutral axis produced by the force acting in tensile area:

$$M_{T,u} = f_{t,u} \frac{\left(l_{eff,c} - x_{c,op}\right)^2}{2}$$

The previous equation is parabolic (see Fig. 21) and can be conveniently rewritten as:

$$M_{op,u} = M_{op,u,max} \left[1 - \left(\frac{N - N_{Mmax}}{N_{m,u}} \right)^2 \right] \tag{32}$$

with

$M_{op,u,max}$: Maximum bending resistance (see Fig. 21):

$$M_{op,u,max} = \frac{l_{eff,c}}{4} N_{m,u}$$

N_{Mmax} : Axial force corresponding to the maximum bending resistance :

$$N_{Mmax} = \frac{N_{C,u} - N_{T,u}}{2}$$

$N_{m,u}$: Average axial resistances :

$$N_{m,u} = \frac{N_{C,u} + N_{T,u}}{2}$$

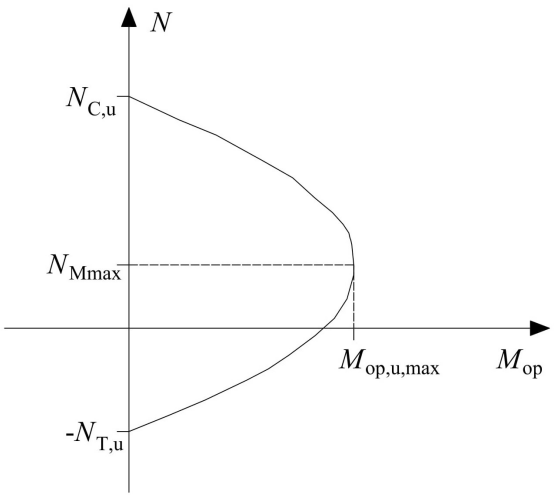

Fig. 21. *Parabolic interaction M-N curve*

The choice of $l_{\text{eff,c}}$ is consistent for the compressive area, but the proposal regarding the tensile area is rather questionable. The lever arm can be underestimated or overestimated (depending on the position of the anchor bolts) and so the maximum bending moment. To avoid these inconsistencies, the contribution of the tensile area to the maximum bending moment is evaluated considering that the tensile resistance develops at the anchor bolts location (see Fig. 22).

The maximum bending moment becomes:

$$M_{\text{op,u,max}} = z_{\text{T,op}} F_{\text{T,u}} + z_{\text{C,op}} F_{\text{c,f,u}} \tag{33}$$

with

$$F_{\text{c,f,u}} = b_{\text{eff,c}} l_{\text{eff,c}} f_{\text{jd,max}} \le b_{\text{fc}} t_{\text{fc}} f_{\text{y,c}}$$

$$z_{\text{T,op}} = w/2$$

$$z_{\text{C,op}} = \frac{l_{\text{eff,c}}}{4}$$

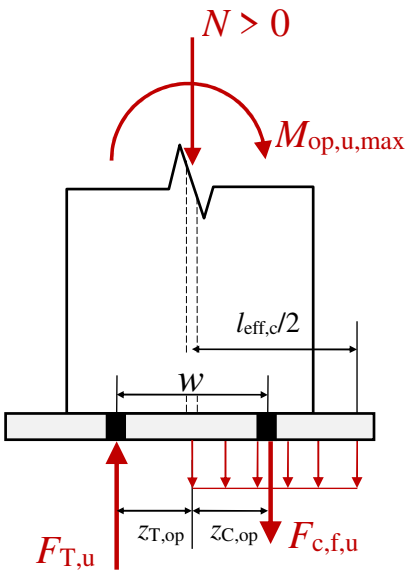

Fig. 22. *Mechanism of internal forces considered for the calculation of* $M_{op,u,max}$

3.3.3. Biaxial bending resistance

The proposed analytical model for the column base plate resistance subjected to an axial force and bending moment in both directions consists in replacing the axial force and bending moments with statically equivalent force distributions acting on both the left and the right sides of the column base-plate. The connection should be sufficiently ductile so the plastic out-of-plane bending resistance can develop at both sides of the connections. The analytical model considers three cases depending on the character of the equivalent axial force (compression or tension) produced by the in-plane bending moment and the axial force. These equivalent forces are applied to both sides of the connection with the out-of-plane bending moments $M_{op,l}$ and $M_{op,r}$ (see Fig. 23). These two bending moments equilibrate the total out-of-plane bending moment applied to the connection:

$$M_{op} = M_{op,r} + M_{op,l} \tag{34}$$

At failure, the resistance is reached in each side of the connection. Considering the proposed parabolic interaction curve in section 3.3.2, the out-of-plane bending moment on each side can be calculated. However for a value of α equal to zero, and thus in presence of pure in-plane bending moment, the out-of-plane bending moment of one side is different from zero. For example in presence of dominant tensile force, the out-of-plane bending moment of the left side, $M_{op,l}$, is equal to zero, but the out-of-plane bending moment of the right side, $M_{op,r}$, is not null. The proposed approach can overestimate

the bending resistance for low values of α. To circumvent this result, the out-of-plane bending moment of the each side will be multiplied by reduction factors χ_r and χ_l on the right and left sides, respectively:

$$\chi_l = \begin{cases} 1, & N < N_{Mmax} \\ \chi_\alpha, & N \geq N_{Mmax} \end{cases} \tag{35}$$

$$\chi_r = \begin{cases} \chi_\alpha, & N < N_{Mmax} \\ 1, & N \geq N_{Mmax} \end{cases} \tag{36}$$

with

$$\chi_\alpha = \frac{\sin\alpha}{\sin\alpha_0} \leq 1 \tag{37}$$

The reduction factor is equal to 1 when failure occurs in the corresponding side under pure in-plane bending moment but to χ_α for the side where failure does not occur for the same loading. The present parametric study didn't investigate low values of α, but experimental tests performed by Bajer et al [12] and numerical study (Seco et al [18], Fasea et al [14]) focused on angles of 26,56 and 30°, respectively. Based on these results, it is proposed to take α_0 equal to $\pi/4$.

The validity domains of the aforementioned loading type are summarized in Table 6. Then, depending on the level of the axial force N and the in-plane bending moment M_{ip}, the model is divided into:

- dominant tensile force (see Fig. 23-a),
- dominant bending moment (see Fig. 23-b),
- dominant compressive force (see Fig. 23-c).

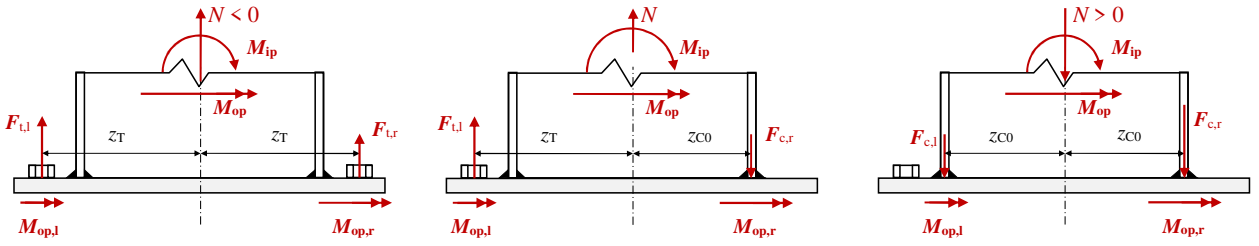

a) Dominant tensile force b) Dominant bending moment c) Dominant compressive force

Fig. 23. *Mechanisms considered in the analytical model for biaxial bending moment*

Table 6 : *Validity range of the mechanisms of the analytical model*

Loading	Range of validity
Dominant tensile force	$N_{\mathrm{T,u}} \le N \le N_{\mathrm{TM}}$, $N_{\mathrm{T,u}} = -2F_{\mathrm{T,u}}$ $-z_{\mathrm{T}} \le e_{\mathrm{N}} = \dfrac{M_{\mathrm{ip}}}{N} \le 0$
Dominant bending moment	$N_{\mathrm{TM}} \le N \le N_{\mathrm{CM}}$ $e_{\mathrm{N}} = \dfrac{M_{\mathrm{ip}}}{N} \ge z_{\mathrm{C0}}$ or $e_{\mathrm{N}} = \dfrac{M_{\mathrm{ip}}}{N} \le -z_{\mathrm{T}}$
Dominant compressive force	$N_{\mathrm{CM}} \le N \le N_{\mathrm{C,u}}$, $N_{\mathrm{C,u}} = 2F_{\mathrm{C,u}}$ $0 \le e_{\mathrm{N}} = \dfrac{M_{\mathrm{ip}}}{N} \le z_{\mathrm{C0}}$
N_{TM} : Boundary between dominant tensile force and dominant bending moment (see section 3.3.3.1) N_{CM} : Boundary between dominant compressive force and dominant bending moment (see section 3.3.3.3)	

3.3.3.1. Dominant tensile force

For the case of a dominant tensile force (see Fig. 23-a), $F_{\mathrm{t,l}}$ and $F_{\mathrm{t,r}}$ produced by the axial force N and the in-plane bending moment M_{ip} are acting on both left and right sides and are obtained as follows:

$$F_{\mathrm{t,l}} = \frac{N}{2} - \frac{M_{\mathrm{ip}}}{2z_{\mathrm{T}}} < 0 \tag{38}$$

$$F_{\mathrm{t,r}} = \frac{N}{2} + \frac{M_{\mathrm{ip}}}{2z_{\mathrm{T}}} \le 0 \tag{39}$$

On the left side, the limit bending moment is:

$$M_{\mathrm{op,l}} = \chi_{\mathrm{l}} \frac{M_{\mathrm{op,u,max}}}{2} \left[1 - \left(\frac{F_{\mathrm{t,l}} - N_{\mathrm{Mmax}}/2}{N_{\mathrm{m,u}}/2} \right)^2 \right] \tag{40}$$

Replacing $F_{\mathrm{t,l}}$ in expression of $M_{\mathrm{op,l}}$, one obtains

$$M_{\mathrm{op,l}} = \chi_{\mathrm{l}} \frac{M_{\mathrm{op,u,max}}}{2} \left[1 - \left(\frac{N - N_{\mathrm{Mmax}} - M_{\mathrm{ip}}/z_{\mathrm{T}}}{N_{\mathrm{m,u}}} \right)^2 \right] \tag{41}$$

On the right side, the limit bending moment is:

$$M_{\mathrm{op,r}} = \chi_{\mathrm{r}} \frac{M_{\mathrm{op,u,max}}}{2} \left[1 - \left(\frac{F_{\mathrm{t,r}} - N_{\mathrm{Mmax}}/2}{N_{\mathrm{m,u}}/2} \right)^2 \right] \tag{42}$$

Inserting $F_{t,r}$ in expression of $M_{op,r}$, one obtains

$$M_{op,r} = \chi_r \frac{M_{op,u,max}}{2}\left[1-\left(\frac{N - N_{Mmax} + M_{ip}/z_T}{N_{m,u}}\right)^2\right] \tag{43}$$

Finally, inserting $M_{op,l}$ and $M_{op,r}$ in M_{op} an expression for the out-of-plane bending resistance is obtained:

$$M_{op} = \chi_l \frac{M_{op,u,max}}{2}\left[1-\left(\frac{N - N_{Mmax} - M_{ip}/z_T}{N_{m,u}}\right)^2\right] + \chi_r \frac{M_{op,u,max}}{2}\left[1-\left(\frac{N - N_{Mmax} + M_{ip}/z_T}{N_{m,u}}\right)^2\right] \tag{44}$$

One can observe that the previous equation can be simplified for $\alpha \geq \alpha_0$:

$$M_{op} = M_{op,u,max}\left[1-\left(\frac{N - N_{Mmax}}{N_{m,u}}\right)^2 - \left(\frac{M_{ip}}{z_T N_{m,u}}\right)^2\right] \tag{45}$$

Thus inserting (1) and (2) in (44), the total bending resistance M_u is obtained by solving the following quadratic equation:

$$a\left(\frac{M}{z_T N_{m,u}}\right)^2 + b_T \frac{M}{z_T N_{m,u}} - c_T = 0 \tag{46}$$

with

$$a = \cos\alpha^2 \delta_\alpha,$$
$$b_T = \sin\alpha \frac{z_T N_{m,u}}{M_{op,u,max}} + \cos\alpha \frac{N - N_{Mmax}}{N_{m,u}}(\chi_r - \chi_l),$$
$$c_T = \delta_\alpha\left[1-\left(\frac{N - N_{Mmax}}{N_{m,u}}\right)^2\right],$$
$$\delta_\alpha = \frac{1+\chi_\alpha}{2}.$$

The total bending resistance for dominant tensile force becomes:

$$M_u = z_T N_{m,u} \chi_T \tag{47}$$

with

$$\chi_T = \frac{\sqrt{b_T^2 + 4ac_T} - b_T}{2a}$$

The limit between the dominant tensile force and dominant bending moment is obtained when the eccentricity is equal to $-z_T$ and thus:

$$M_{ip} = -Nz_T \tag{48}$$

Inserting Equations (1), (2) and (48) in (44), we get the axial force that boarder the two domains:

$$N_{TM} = N_{m,u} \frac{\sqrt{b_{TM}^2 + 8\chi_l c_{TM}} + b_{TM}}{4\chi_l} \tag{49}$$

with

$$b_{TM} = \tan\alpha \frac{z_T N_{m,u}}{M_{op,u,max}} + 2\chi_l \frac{N_{M\,max}}{N_{m,u}},$$

$$c_{TM} = \delta_\alpha \left[1 - \left(\frac{N_{Mmax}}{N_{m,u}}\right)^2\right].$$

3.3.3.2. Dominant bending moment

In presence of dominant bending moment (see Fig. 23-b), the tensile force applied on the left side $F_{t,l}$ and the compressive force on the right side $F_{c,r}$, can be obtained with:

$$F_{t,l} = \frac{\alpha_l N}{2} - \frac{M_{ip}}{2\bar{z}} \le 0 \tag{50}$$

$$F_{c,r} = \frac{\alpha_r N}{2} + \frac{M_{ip}}{2\bar{z}} \ge 0 \tag{51}$$

with $\bar{z} = \frac{z_{C0} + z_T}{2}$, $\alpha_l = \frac{z_{C0}}{\bar{z}}$, $\alpha_r = \frac{z_T}{\bar{z}}$.

These forces applied on each side of the connection concomitantly with the out-of-plane bending moments $M_{op,l}$ and $M_{op,r}$, and the ultimate limit state is reached on both sides.

Again, considering the parabolic interaction curve, the limit for the out-of-plane bending moments are:

On the left side:

$$M_{op,l} = \chi_l \frac{M_{op,u,max}}{2}\left[1 - \left(\frac{F_{t,l} - N_{Mmax}/2}{N_{m,u}/2}\right)^2\right] \tag{52}$$

On the right side:

$$M_{\mathrm{op,r}} = \chi_{\mathrm{r}} \frac{M_{\mathrm{op,u,max}}}{2}\left[1-\left(\frac{F_{\mathrm{c,r}} - N_{\mathrm{Mmax}}/2}{N_{\mathrm{m,u}}/2}\right)^2\right] \tag{53}$$

Inserting $F_{\mathrm{t,l}}$ and $F_{\mathrm{c,r}}$ in $M_{\mathrm{op,l}}$ and $M_{\mathrm{op,r}}$ respectively, one obtains:

On the left side:

$$M_{\mathrm{op,l}} = \chi_{\mathrm{l}} \frac{M_{\mathrm{op,u,max}}}{2}\left[1-\left(\frac{\alpha_{\mathrm{l}} N - N_{\mathrm{Mmax}} - M_{\mathrm{ip}}/\bar{z}}{N_{\mathrm{m,u}}}\right)^2\right] \tag{54}$$

On the right side:

$$M_{\mathrm{op,r}} = \chi_{\mathrm{r}} \frac{M_{\mathrm{op,u,max}}}{2}\left[1-\left(\frac{\alpha_{\mathrm{r}} N - N_{\mathrm{Mmax}} + M_{\mathrm{ip}}/\bar{z}}{N_{\mathrm{m,u}}}\right)^2\right] \tag{55}$$

Finally, inserting $M_{\mathrm{op,l}}$ and $M_{\mathrm{op,r}}$ in M_{op} an expression for the out-of-plane bending resistance is obtained:

$$M_{\mathrm{op}} = \chi_{\mathrm{l}} \frac{M_{\mathrm{op,u,max}}}{2}\left[1-\left(\frac{\alpha_{\mathrm{l}} N - N_{\mathrm{Mmax}} - M_{\mathrm{ip}}/\bar{z}}{N_{\mathrm{m,u}}}\right)^2\right] + \chi_{\mathrm{r}} \frac{M_{\mathrm{op,u,max}}}{2}\left[1-\left(\frac{\alpha_{\mathrm{r}} N - N_{\mathrm{Mmax}} + M_{\mathrm{ip}}/\bar{z}}{N_{\mathrm{m,u}}}\right)^2\right] \tag{56}$$

One can observe that the previous equation can be simplified for $\alpha \geq \alpha_0$:

$$M_{\mathrm{op}} = M_{\mathrm{op,u,max}}\left[1-\frac{1}{2}\left(\frac{\alpha_{\mathrm{l}} N - N_{\mathrm{Mmax}} - M_{\mathrm{ip}}/\bar{z}}{N_{\mathrm{m,u}}}\right)^2 - \frac{1}{2}\left(\frac{\alpha_{\mathrm{r}} N - N_{\mathrm{Mmax}} + M_{\mathrm{ip}}/\bar{z}}{N_{\mathrm{m,u}}}\right)^2\right] \tag{57}$$

The total bending resistance M_{u} is obtained by solving the following quadratic equation:

$$a\left(\frac{M_{\mathrm{u}}}{\bar{z}N_{\mathrm{m,u}}}\right)^2 + b_{\mathrm{M}}\frac{M_{\mathrm{u}}}{\bar{z}N_{\mathrm{m,u}}} - c_{\mathrm{M}} = 0 \tag{58}$$

with

$$a = \cos\alpha^2 \delta_\alpha$$

$$b_M = \sin\alpha \frac{\bar{z} N_{m,u}}{M_{op,u,max}} + \cos\alpha \left[\frac{N}{N_{m,u}} (\alpha_r \chi_r - \alpha_l \chi_l) + \frac{N_{Mmax}}{N_{m,u}} (\chi_l - \chi_r) \right]$$

$$c_M = \delta_\alpha - \frac{\chi_r}{2} \left(\frac{\alpha_r N - N_{Mmax}}{N_{m,u}} \right)^2 - \frac{\chi_l}{2} \left(\frac{\alpha_l N - N_{Mmax}}{N_{m,u}} \right)^2 .$$

The positive solution of this equation comes:

$$M_u = \bar{z} N_{m,u} \chi_M \tag{59}$$

with

$$\chi_M = \frac{\sqrt{b_M^2 + 4ac_M} - b_M}{2a}$$

3.3.3.3. Dominant compressive force

In presence of dominant compressive force (see Fig. 23-c), the equivalent forces $F_{c,l}$ and $F_{c,r}$, resulting from the applied axial load N and the in-plane bending moment M_{ip} are calculated from:

$$F_{c,l} = \frac{N}{2} - \frac{M_{ip}}{2z_{C0}} \geq 0 \tag{60}$$

$$F_{c,r} = \frac{N}{2} + \frac{M_{ip}}{2z_{C0}} > 0 \tag{61}$$

These forces are applied on each side of the connection concomitantly with the out-of-plane bending moments $M_{op,l}$ and $M_{op,r}$ and failure is reached on each side. Again, considering the parabolic interaction curve and reduction factors χ_l and χ_r, the limit out-of-plane bending moments are:

on the left side:

$$M_{op,l} = \chi_l \frac{M_{op,u,max}}{2} \left[1 - \left(\frac{F_{c,l} - N_{Mmax}/2}{N_{m,u}/2} \right)^2 \right] \tag{62}$$

on the right side:

$$M_{op,r} = \chi_r \frac{M_{op,u,max}}{2} \left[1 - \left(\frac{F_{c,r} - N_{Mmax}/2}{N_{m,u}/2} \right)^2 \right] \tag{63}$$

Inserting equation of $F_{c,l}$ and $F_{c,r}$ in $M_{op,l}$ and $M_{op,r}$ respectively it is obtained:

on the left side:

$$M_{\mathrm{op,l}} = \chi_{\mathrm{l}} \frac{M_{\mathrm{op,u,max}}}{2} \left[1 - \left(\frac{N - N_{\mathrm{Mmax}} - M_{\mathrm{ip}} / z_{\mathrm{C0}}}{N_{\mathrm{m,u}}} \right)^2 \right] \tag{64}$$

on the right side:

$$M_{\mathrm{op,r}} = \chi_{\mathrm{r}} \frac{M_{\mathrm{op,u,max}}}{2} \left[1 - \left(\frac{N - N_{\mathrm{Mmax}} + M_{\mathrm{ip}} / z_{\mathrm{C0}}}{N_{\mathrm{m,u}}} \right)^2 \right] \tag{65}$$

Finally, inserting $M_{\mathrm{op,l}}$ and $M_{\mathrm{op,r}}$ in M_{op} an expression for the out-of-plane bending resistance is obtained:

$$M_{\mathrm{op}} = \chi_{\mathrm{l}} \frac{M_{\mathrm{op,u,max}}}{2} \left[1 - \left(\frac{N - N_{\mathrm{Mmax}} - M_{\mathrm{ip}} / z_{\mathrm{C0}}}{N_{\mathrm{m,u}}} \right)^2 \right] + \chi_{\mathrm{r}} \frac{M_{\mathrm{op,u,max}}}{2} \left[1 - \left(\frac{N - N_{\mathrm{Mmax}} + M_{\mathrm{ip}} / z_{\mathrm{C0}}}{N_{\mathrm{m,u}}} \right)^2 \right] \tag{66}$$

One can observe that the previous equation can be simplified for $\alpha \geq \alpha_0$:

$$M_{\mathrm{op}} = M_{\mathrm{op,u,max}} \left[1 - \left(\frac{N - N_{\mathrm{Mmax}}}{N_{\mathrm{m,u}}} \right)^2 - \left(\frac{M_{\mathrm{ip}}}{z_{\mathrm{C0}} N_{\mathrm{m,u}}} \right)^2 \right] \tag{67}$$

The total bending resistance M_{u} is obtained by solving a quadratic equation as follows:

$$a \left(\frac{M_{\mathrm{u}}}{z_{\mathrm{C0}} N_{\mathrm{m,u}}} \right)^2 + b_{\mathrm{C}} \frac{M_{\mathrm{u}}}{z_{\mathrm{C0}} N_{\mathrm{m,u}}} - c_{\mathrm{C}} = 0 \tag{68}$$

with

$$a = \cos\alpha^2 \delta_{\alpha},$$

$$b_{\mathrm{C}} = \sin\alpha \frac{z_{\mathrm{C0}} N_{\mathrm{m,u}}}{M_{\mathrm{op,u,max}}} + \cos\alpha \frac{N - N_{\mathrm{M\,max}}}{N_{\mathrm{m,u}}} \left(\chi_{\mathrm{r}} - \chi_{\mathrm{l}} \right),$$

$$c_{\mathrm{C}} = \delta_{\alpha} \left[1 - \left(\frac{N - N_{\mathrm{Mmax}}}{N_{\mathrm{m,u}}} \right)^2 \right]$$

The positive solution of this equation is:

$$M_{\mathrm{u}} = z_{\mathrm{C0}} N_{\mathrm{m,u}} \chi_{\mathrm{C}} \tag{69}$$

with

$$\chi_{\mathrm{C}} = \frac{\sqrt{b_{\mathrm{C}}^2 + 4ac_{\mathrm{C}}} - b_{\mathrm{C}}}{2a}$$

The limit between the dominant compressive force and dominant bending moment is obtained when the eccentricity is equal to z_{C} and thus:

$$M_{\mathrm{ip}} = N z_{\mathrm{C0}} \tag{70}$$

Inserting Equations (1), (2) and (70) in (66), we get the axial force between these two domains:

$$N_{\mathrm{CM}} = N_{\mathrm{m,u}} \frac{\sqrt{b_{\mathrm{CM}}^2 + 8\chi_{\mathrm{r}} c_{\mathrm{CM}}} - b_{\mathrm{CM}}}{4\chi_{\mathrm{r}}} \tag{71}$$

with

$$b_{\mathrm{CM}} = \tan\alpha \frac{z_{\mathrm{C0}} N_{\mathrm{m,u}}}{M_{\mathrm{op,u,max}}} - 2\chi_{\mathrm{r}} \frac{N_{\mathrm{Mmax}}}{N_{\mathrm{m,u}}},$$

$$c_{\mathrm{CM}} = \delta_{\alpha} \left[1 - \left(\frac{N_{\mathrm{Mmax}}}{N_{\mathrm{m,u}}} \right)^2 \right].$$

3.3.3.4. General formulation and simplified method

From the previous development, a general equation of the bending resistance can be expressed as a function of the lever arm of the right and left sides (respectively z_{r} and z_{l}), the average lever arm, $\bar{z}$, and the ratio α_{r} and α_{l} :

$$\alpha_{\mathrm{l}} = \frac{z_{\mathrm{r}}}{\bar{z}} \tag{72}$$

$$\alpha_{\mathrm{r}} = \frac{z_{\mathrm{l}}}{\bar{z}}. \tag{73}$$

The lever arms depend of the loading conditions involved by the in-plane bending moment and are given in Table 7.

Table 7 : *Lever arms*

Loading	Condition	Lever arm
Dominant tensile force	$N_{T,u} \le N < N_{TM}$	$z_l = z_r = z_T$
Dominant bending moment	$N_{TM} \le N \le N_{CM}$	$z_l = z_T,\ z_r = z_{C0}$
Dominant compressive force	$N_{CM} < N \le N_{C,u}$	$z_l = z_r = z_{C0}$

Finally, the bending resistance is:

$$M_u = \bar{z} N_{m,u} \chi_{M_u} \ge M_{op,u} \tag{74}$$

with

$$\chi_{M_u} = \frac{\sqrt{b^2 + 4ac} - b}{2a}$$

$$a = \cos\alpha^2 \delta_\alpha$$

$$b = \sin\alpha \frac{\bar{z} N_{m,u}}{M_{op,u,max}} + \cos\alpha \left[\frac{N}{N_{m,u}} \left(\alpha_r \chi_r - \alpha_l \chi_l \right) + \frac{N_{Mmax}}{N_{m,u}} \left(\chi_l - \chi_r \right) \right]$$

$$c = \delta_\alpha - \frac{\chi_r}{2} \left(\frac{\alpha_r N - N_{Mmax}}{N_{m,u}} \right)^2 - \frac{\chi_l}{2} \left(\frac{\alpha_l N - N_{Mmax}}{N_{m,u}} \right)^2 .$$

The M-N interaction curves calculated for connections P1 and P3 respectively composed of HEA 200 and IPE 200 are depicted in Fig. 24. For values of α lower or equal to 45°, the curves are almost parabolic. The curve is multi-linear when α is null and thus for in-plane bending moment. This shape is clearly in line with the Eurocode 3 method for column base plates [8]. For values of α comprise between 0 and 30°, the curves are in between these two shapes: parabolic and multilinear. The proposed expression of the bending moment is able to capture the interaction in presence of uniaxial bending moment (in-plane and out-of-plane) but also for biaxial bending moment.

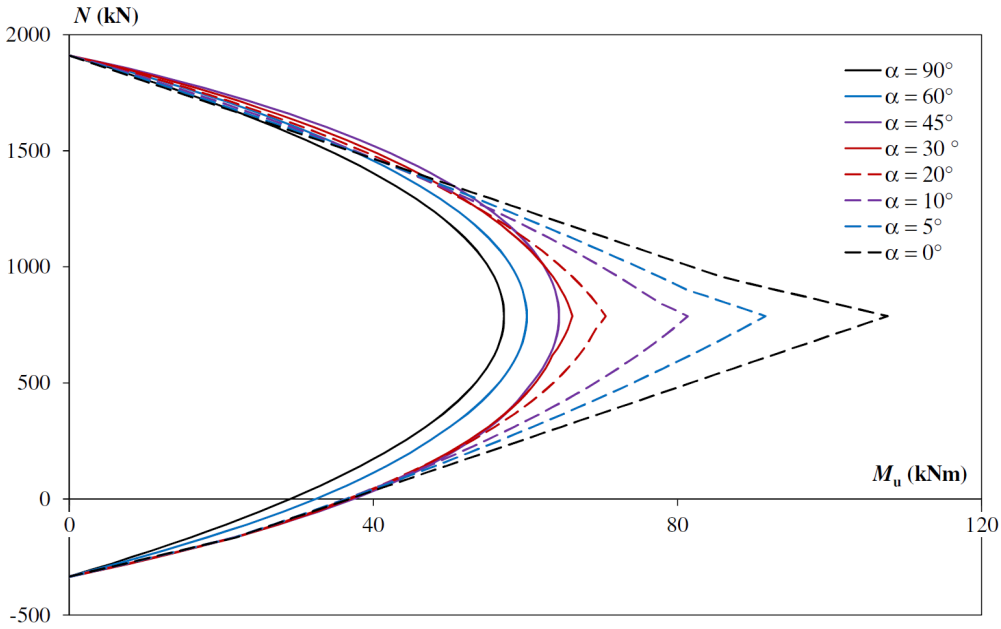

a) Connection P1

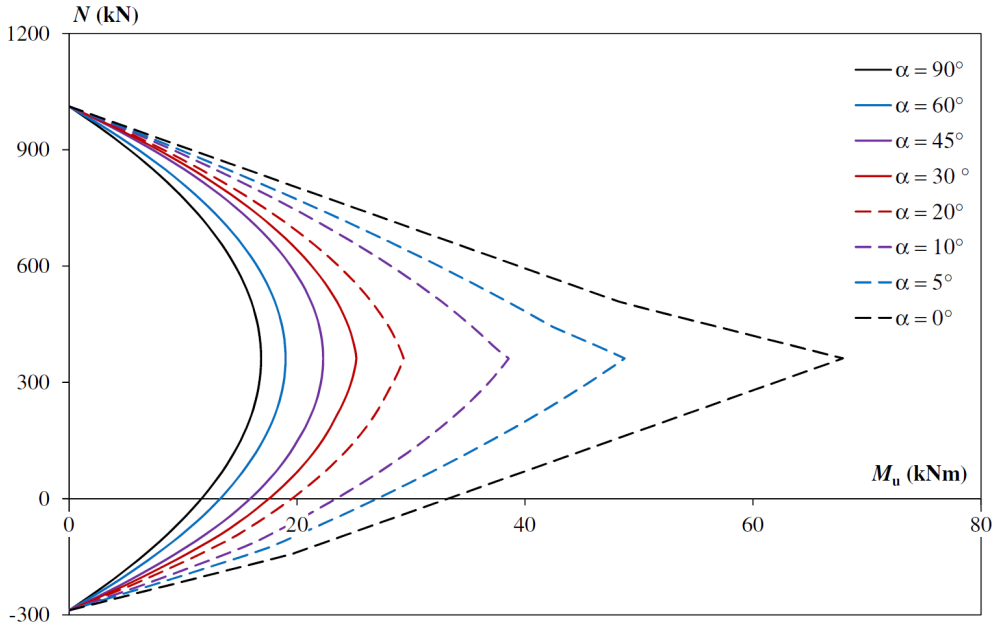

b) Connection P3

Fig. 24. *M-N interaction curves*

However simplifications are necessary to ease the application of the proposed formulation. From numerical simulations and the application of the proposed analytical model, we can observe that the bending moment is maximal when the axial force is equal to the N_{Mmax} whatever the value of the angle α. In addition, the curves are almost parabolic for α greater that 35°.

Based on these observations, it is proposed to estimate the M-N curves by the following expression:

$$M_{\mathrm{u}} = M_{\mathrm{u,max}} \left[1 - \left(\frac{\left| N - N_{\mathrm{Mmax}} \right|}{N_{\mathrm{m,u}}} \right)^{n} \right] \tag{75}$$

where

$$n = 1 + \frac{\alpha}{35} \leq 2 \tag{76}$$

$M_{\mathrm{u,max}}$ is the maximal bending moment for a given value of α :

$$M_{\mathrm{u,max}} = \chi_{\mathrm{M_{u,max}}} M_{\mathrm{ip,u,max}} \tag{77}$$

with

$$\chi_{\mathrm{M_{u,max}}} = \frac{\sqrt{\overline{M}^{2} + 1} - \overline{M}}{\cos\alpha} \geq \frac{M_{\mathrm{op,u,max}}}{M_{\mathrm{ip,u,max}}}$$

$$\overline{M} = \frac{M_{\mathrm{ip,u,max}}}{M_{\mathrm{op,u,max}}} \frac{\tan\alpha}{2\delta_{\alpha}}$$

$M_{\mathrm{ip,u,max}}$: Maximal in-plane bending resistance calculated for $N = N_{\mathrm{Mmax}}$:

$$M_{\mathrm{ip,u,max}} = \frac{z_{\mathrm{T}} N_{\mathrm{T,u}} + z_{\mathrm{C0}} N_{\mathrm{C,u}}}{2} \tag{78}$$

The M-N interaction curves calculated with the analytical model and the simplified method are depicted in Fig. 25 for connections P1 and P3. The curves of the simplified method and analytical model are identical for α equal to 90°. The resistance obtained by the simplified method are lower than those calculated by the analytical model in presence of pure in-place bending moment and for $N < N_{\mathrm{Mmax}}$ contrary to what is observed for $N > N_{\mathrm{Mmax}}$. For greater value of α, the simplified method overestimate slightly the maximum bending moment (for $N = N_{\mathrm{Mmax}}$). However, the comparison with numerical simulations presented in section 3.5 demonstrate that the proposed method is conservative.

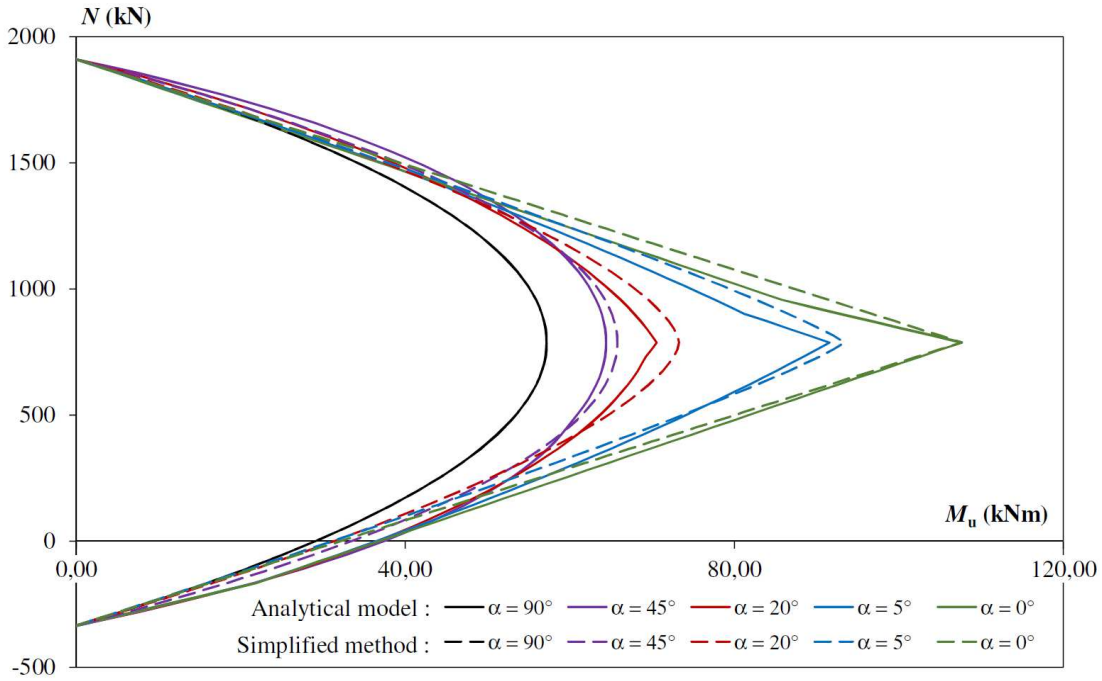

a) Connection P1

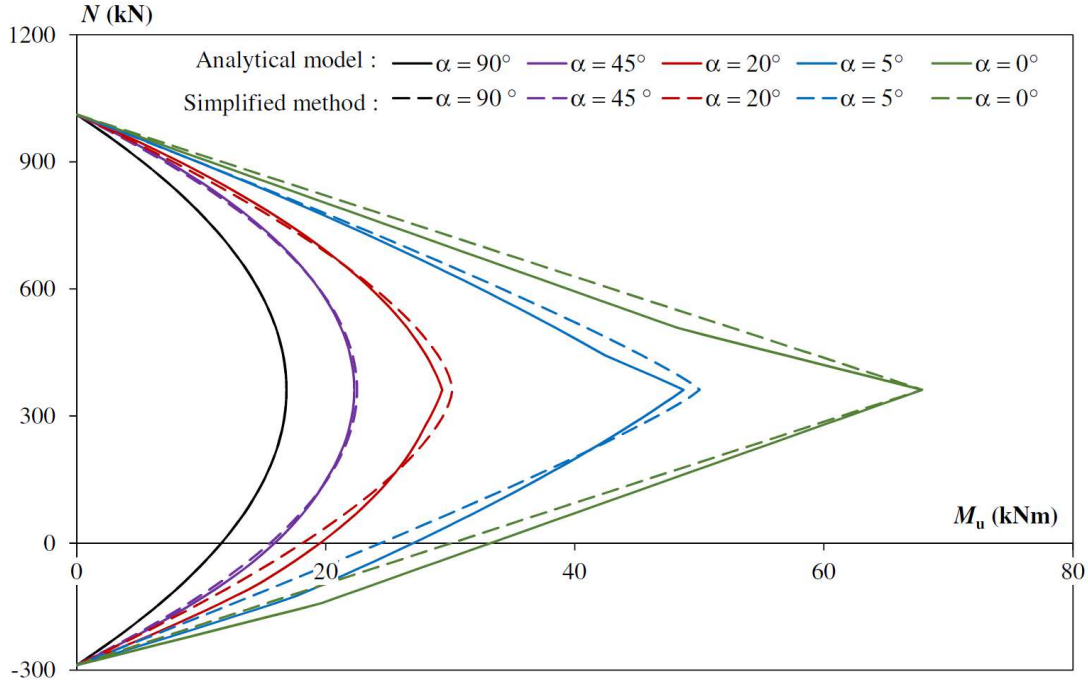

b) Connection P3

Fig. 25. *M-N interaction curves : comparison between analytical model and simplified method*

3.4. Comparison to experimental tests

The bending moment resistances calculated with the analytical model and the simplified method (with Equations (74) and (75), respectively) are compared against results of experimental tests carried out by Seco et al [18] and by Bajer et al [12]. The ultimate bending moment resistances as well as the ra-

tio between the experimental and analytical results are given in Table 8. In absence of mechanical characterisation performed by Bajer et al [12], the yield strength and ultimate tensile strength of steel of the base-plate are assumed equal to 340 and 500 N/mm^2 respectively. The ultimate tensile strength of anchor bolts taken equal to 898 N/mm^2 is determined based on the tensile force measured at failure during tests [12].

Table 8 : *Comparison of analytical results against tests and numerical simulations*

Reference	Specimen	α (°)	N (kN)	Experimental	Analytical		Simplified method	
				$M_{j,u,exp}$ (kNm)	$M_{j,u,ana}$ (kNm)	Ana/Exp	$M_{j,u,meth}$ (kNm)	Meth/Exp
Seco et al [18]	SPE1-M0	0	0	43,2	43,6	1,01	34,5	0,80
	SPE2-M0	0	0	48,5	50,1	1,03	38,1	0,79
	SPE1-M90	90	0	33,3	32,7	0,98	32,7	0,98
	SPE2-M90	90	0	40,2	37,0	0,92	37,0	0,92
	SPE1-M45	45	0	39,4	41,5	1,05	36,9	0,94
	SPE2-M45	45	0	47,3	46,2	0,98	41,2	0,87
Bajer et al [12]	Joints 1/2	0	400	189	175	0,93	144,4	0,76
	Joints 3/4	26,56	400	169	135	0,80	129,3	0,76

The results presented above show a good agreement between the experimental tests and the predictions of the proposed analytical model for the estimation of the bending resistance of column base plates for in-plane, out-of-plane and biaxial bending moments. For SPE2-M0 and SPE1-M45, the resistances are overestimated with an error of approximatively 5%, which is considered as an acceptable value for the unsafe side (<10%). For SPE1-M90 and SPE2-M90, the proposed model predict the resistance on the safe side with an error of 2% and 8%, respectively. The mean value of the ratio $M_{j,u,ana}/M_{j,u,exp}$ is equal to 0,96. The simplified method is more conservative than the analytical model particularly in presence of in-plane bending moment. It can be explained by the fact that the centre of compression is positioned at the centre of the column flange. The results are improved when α increases. The results obtained by the analytical model and the simplified method are logically identical in presence of pure out-of-plane bending moment ($\alpha = \pi/2$).

3.5. Comparison to numerical results

The *M-N* interaction curves for in-plane bending moment predicted by the analytical model of section 3.3.1, the design method (see section 3.3.3.4) and Eurocode 3 are compared in Fig. 26 against the results of the parametric study. In addition, the resistance obtained analytically are compared to numerical results of Seco et al [18] for angles of 30 and 60° in Table 9.

Table 9 : *Comparison of analytical results against numerical simulations*

Reference	Specimen	α (°)	N (kN)	Numerical	Analytical		Simplified method	
				$M_{j,u,num}$ (kNm)	$M_{j,u,ana}$ (kNm)	Ana/Num	$M_{j,u,meth}$ (kNm)	Meth/Num
Seco et al [18]	SPE1-M30	30	0	39,2	40,6	1,04	36,1	0,92
	SPE2-M30	30	0	49,4	44,9	0,91	42,1	0,85
	SPE1-M60	60	0	37,0	36,3	0,98	34,5	0,93
	SPE2-M60	60	0	43,3	40,8	0,94	38,7	0,89

In most cases, the resistance obtained by the analytical models is lower than the numerical resistances and so the models can be used with confidence as predictions are mostly on the safe side. The analytical and numerical model are in better agreement when failure occurs by anchor bolt rupture in tension than by column yielding/buckling. This fact is related to the complexity of the characterization of the connection behavior under high compressive force and also to the development of strain hardening on the column neglected in the proposed analytical model. However the shape of analytical curve is similar to the numerical one's even for high compressive force. The Eurocode 3 approach is conservative whatever the magnitude of the axial force.

The comparison of the numerically predicted interaction curves for out-of-plane bending moment against the analytical interaction curves (see Fig. 27) allow to conclude the suitability of the parabolic interaction approach used. Except for specimens P1 and P4, in which the resistance is slightly overestimated, the analytical curves are circumscribed by the numerical interaction curves. The bending moment resistances estimated with the design model procedure for biaxial bending moment are also compared against the results obtained with the numerical model in Fig. 28. The values obtained by the analytical models generally underestimate the resistances obtained by the FE analysis.

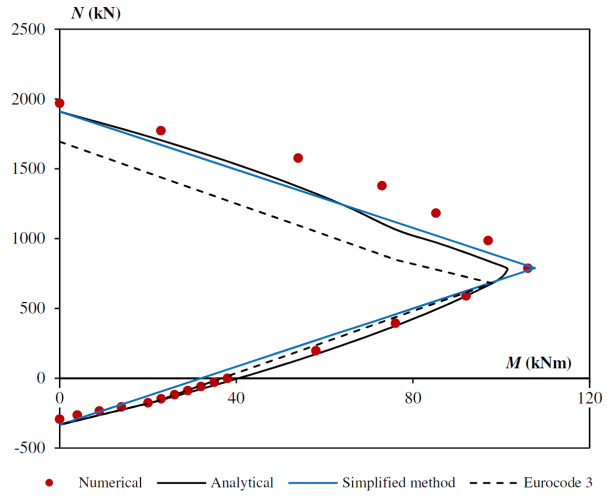

a) Specimen P1

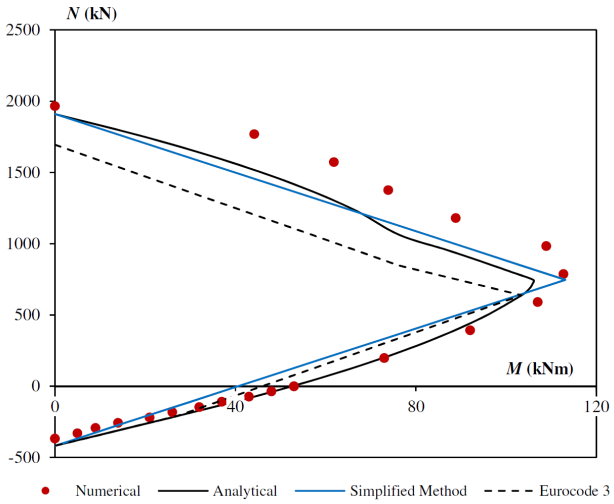

b) Specimen P2

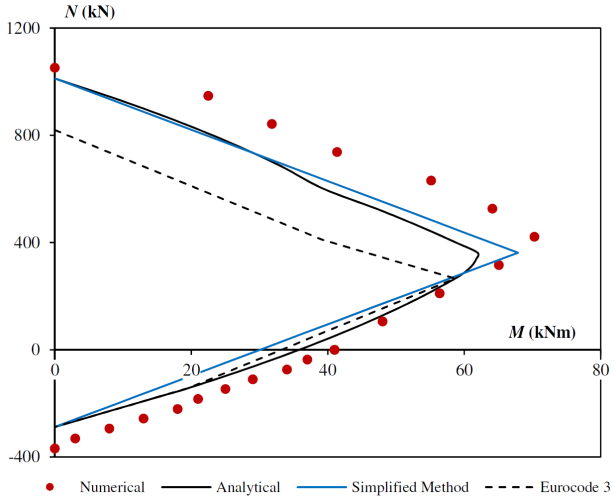

c) Specimen P3

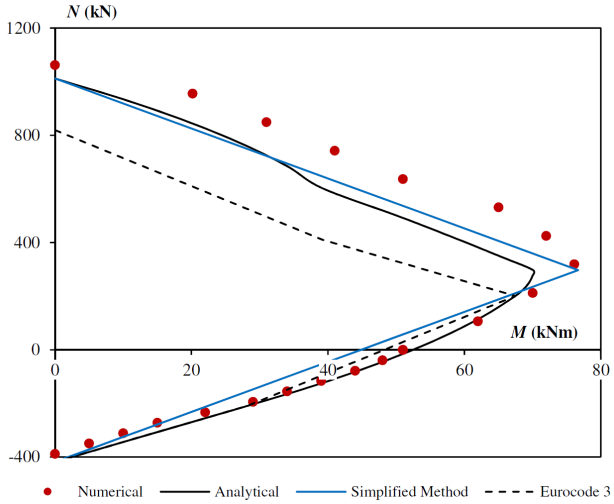

d) Specimen P4

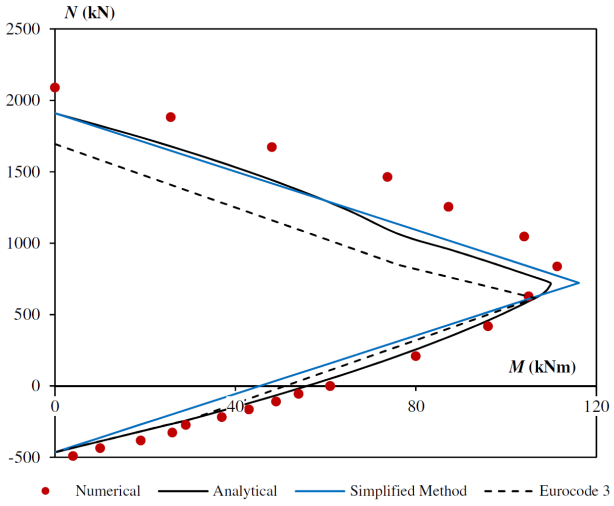

e) Specimen P5

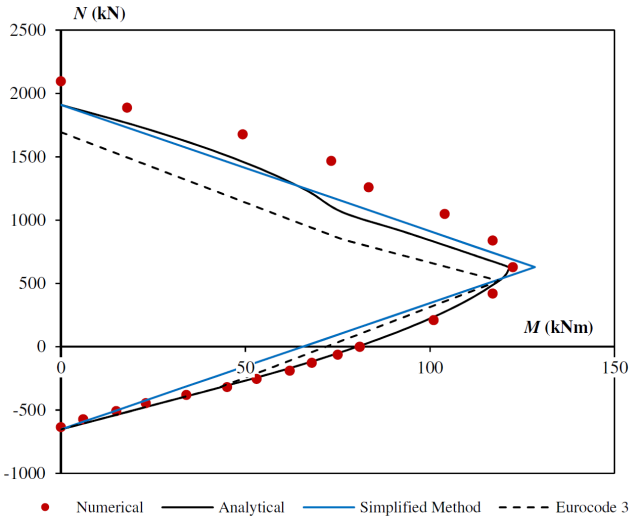

f) Specimen P6

Fig. 26. *M-N interaction curves for in-plane bending moment*

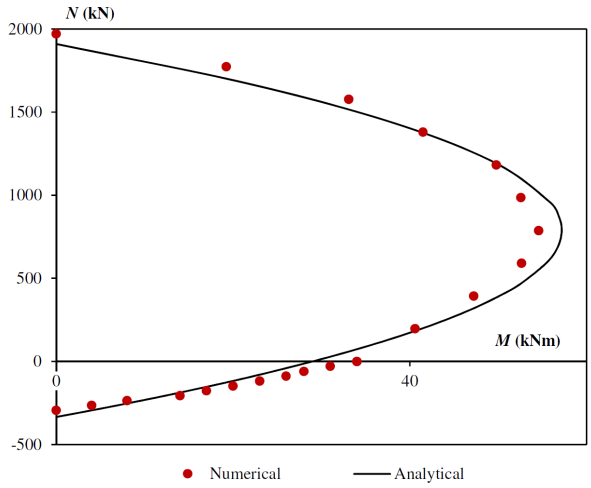

a) Specimen P1

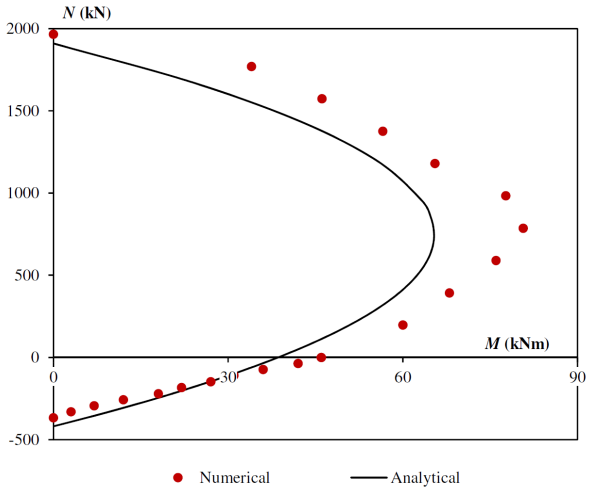

b) Specimen P2

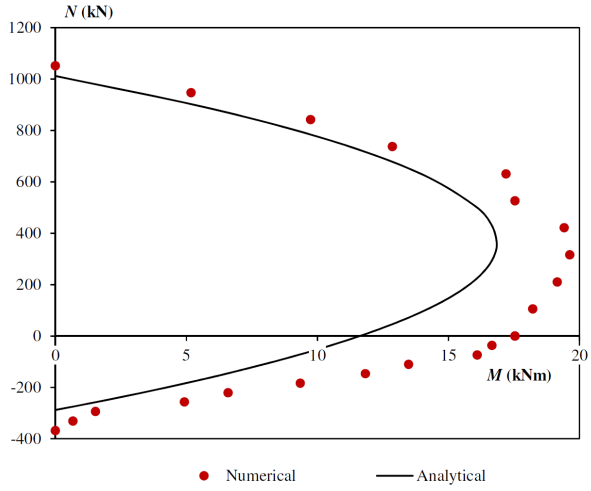

c) Specimen P3

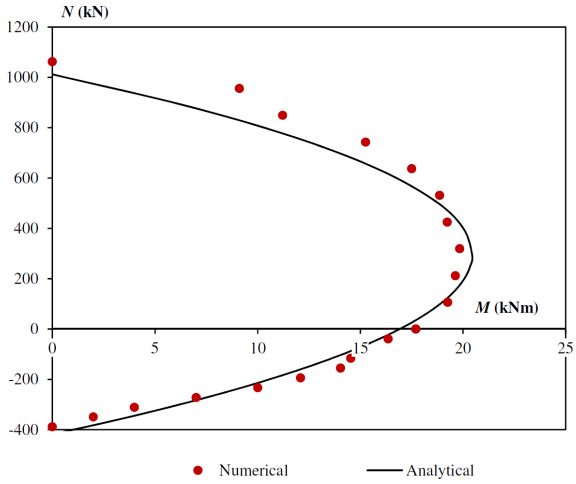

d) Specimen P4

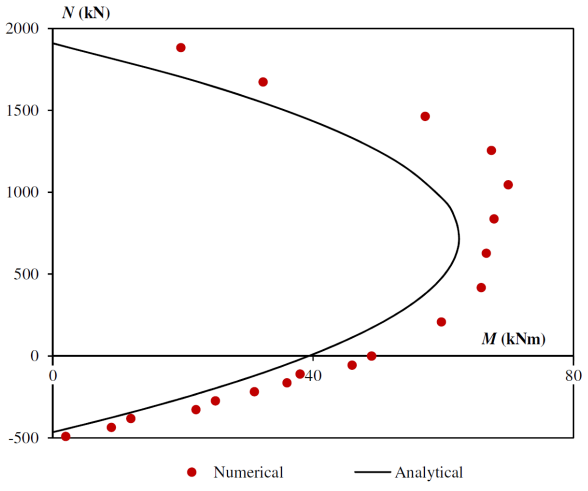

e) Specimen P5

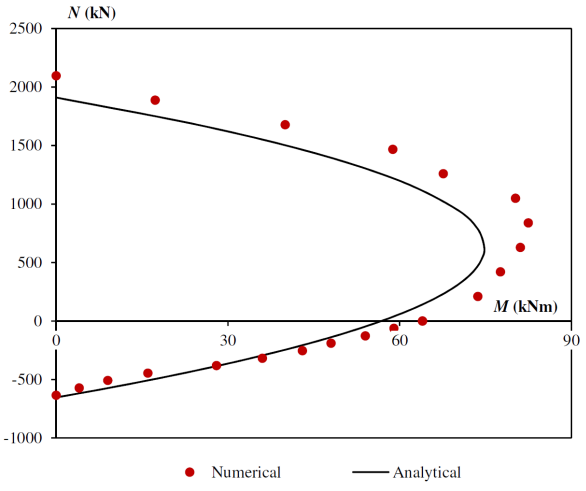

f) Specimen P6

Fig. 27. *M-N interaction curves for out-of-plane bending moment*

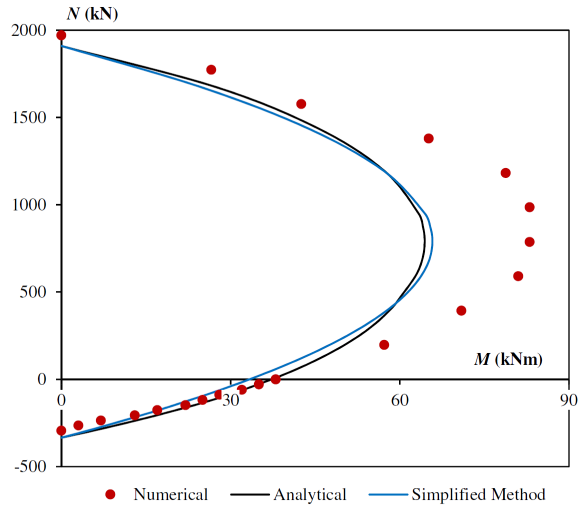

a) Specimen P1

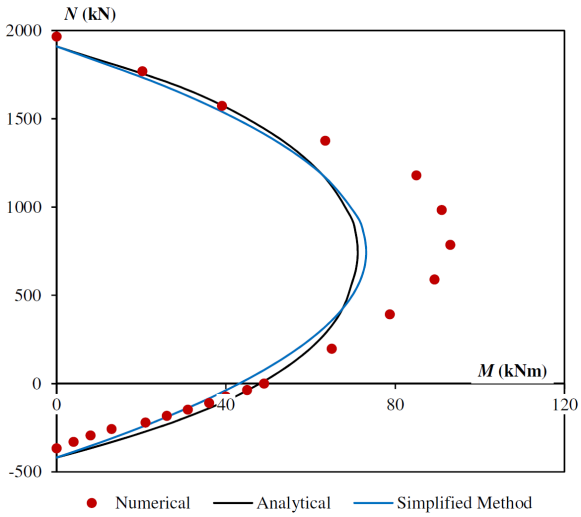

b) Specimen P2

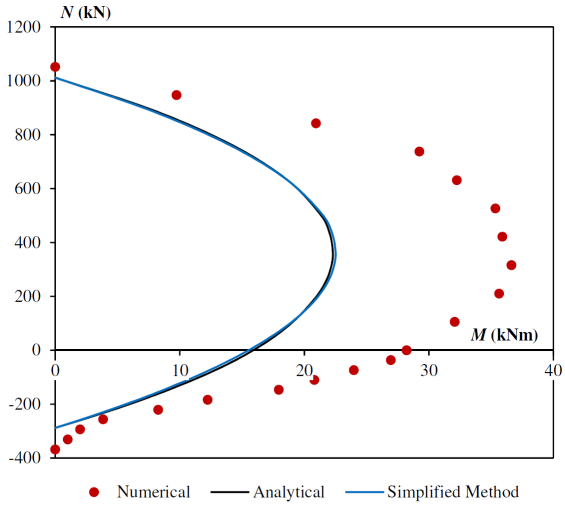

c) Specimen P3

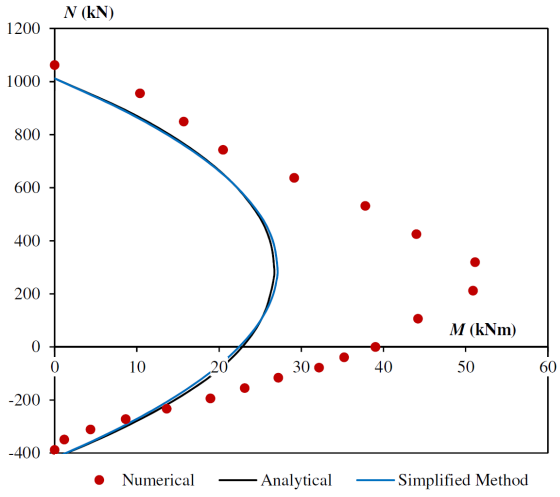

d) Specimen P4

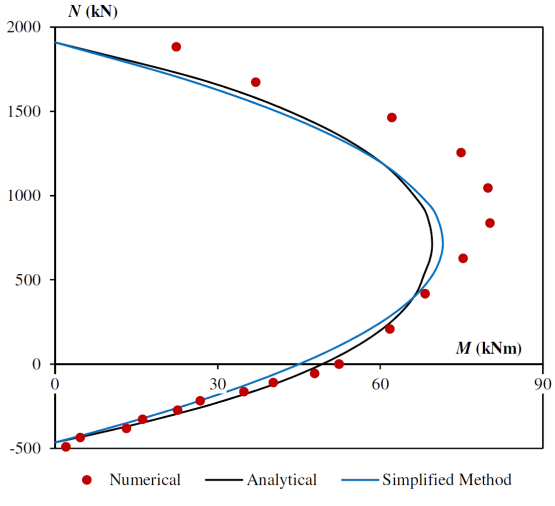

e) Specimen P5

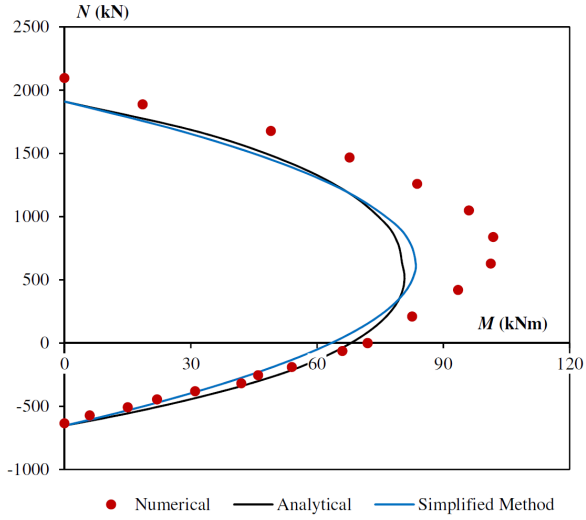

f) Specimen P6

Fig. 28. *M-N interaction curves for biaxial bending moment (α = 45°)*

Looking carefully at the interaction curves at collapse depicted in Fig. 26 to Fig. 28, it can be observed that the analytical curves are generally circumscribed by the numerical curves, revealing a good accuracy of the obtained results with an acceptable safety margin, except for specimens P3 and P4.

In addition, the M_{op}-M_{ip} interaction curves obtained with the analytical model are compared to numerical results of Fasae et al [14] in Fig. 29 for different values of the axial force. The lever arm z_{C0} is replaced by z_C calculated with Eq (14). For low values of the axial force, the analytical model is in very good agreement with numerical results. For greater values of the axial force and low values of α, the analytical model is quite conservative as a result of the reduction coefficient given by Equation (37) that should probably be relaxed in presence of high compressive force.

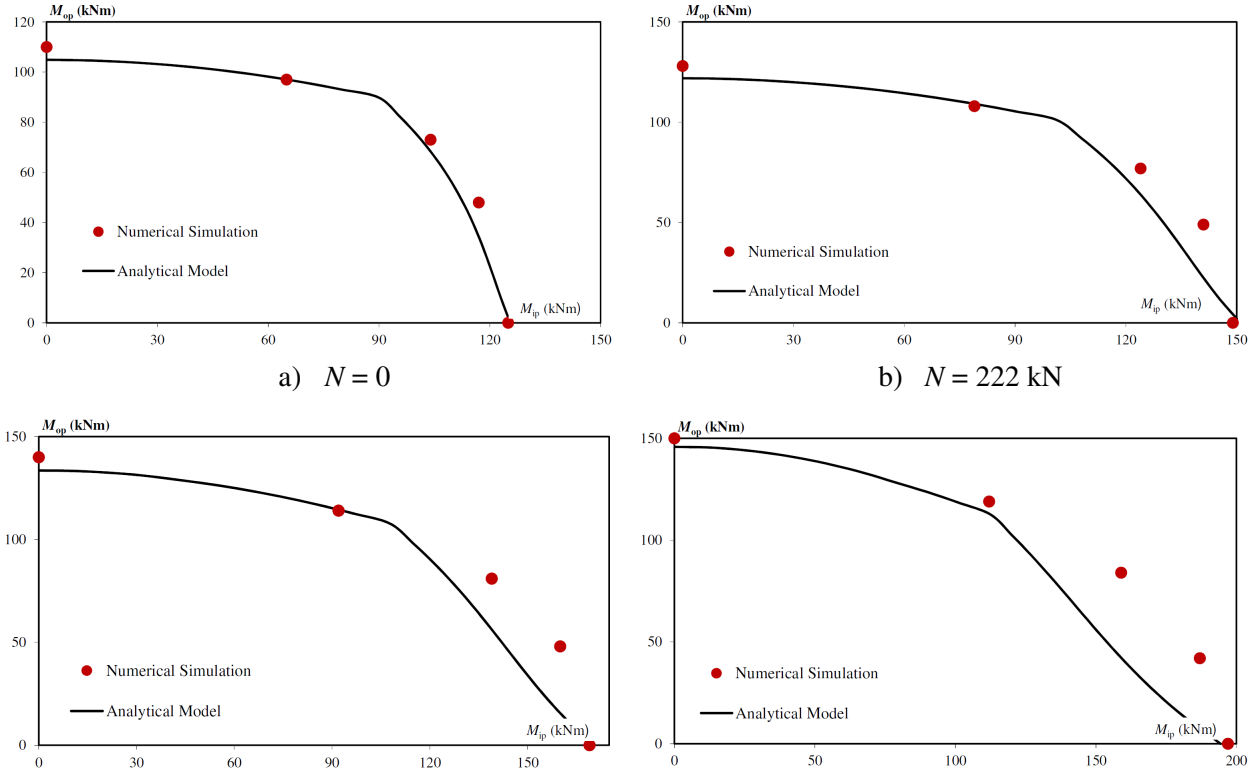

Fig. 29. Interaction curves M_{ip}-M_{op} compared to results of Fasae et al [14]

4. CONCLUSIONS

In the present paper, a finite element model of exposed column base plate subjected to the combination of an axial force and uniaxial (in-plane and out-of-plane) or biaxial bending moments (with an angle of 45°), previously validated against experimental tests [18], has been developed in Abaqus and used to perform an extensive parametric study. This parametric study permit to highlight the impact of base-plate thickness, anchor bolt diameter, column section geometry on the behaviour of this type of connection. The main conclusions of this parametric study are the following:

- In presence of tensile force, the failure mode is not impacted by the orientation of the bending moment axis and corresponds to anchor bolt rupture in tension. Increasing the tensile force results in a decrease of both the bending resistance and the initial rotational stiffness regardless of the orientation of the bending moment,
- For high compressive force (greater than half the compressive resistance of the connection), the failure was due to the column buckling occurring after major yielding. The resistance decrease with increasing value of the axial force. For compressive force lower than half of the compressive resistance, the failure mode corresponds to anchor bolt rupture in tension for in-plane and biaxial bending moments (for an angle of 45°). On the contrary, failure develop in the column in presence of out-of-plane bending moment mainly due to high stress concentration in the compressed flange.
- The shape of the M-N curve is parabolic for out-of-plane bending moment and multi-linear for in-plane bending moment. For biaxial bending moment with an angle of 45°, the curve is in between.
- The resistance and initial rotational stiffness increase with the increase of the base-plate thickness and the anchor bolt diameter.
- In presence of pure bending moment, contact pressure distribution develop at the outer edge of the base plate for thicker one and closer to the column flange for thinner one. For the maximum bending moment, contact pressure develop entirely around the column flange. The ex-

tent of the contact area is greater for thick base plate and the fillet welds contribute to diffuse the compression force directly to the concrete block.

Based on these observations, analytical models have been proposed to evaluate the bending resistances of exposed column base plates regardless of the orientation of the bending moment axis. The extent of the contact area depends on the base-plate thickness and is based on the additional bearing width of Eurocode 3 improved to consider the development of a plastic bending moment in the base plate and the contribution of fillet welds. The column components in compression are directly integrated to the bearing strength. For in-plane bending moment, the contribution of the web in compression is added to that of the flange. Moreover, the tensile force reduces when more than half of the beam web is under compression as observed in numerical simulations. For out-of-plane bending moment, a parabolic interaction curve is considered based on a simple statically equivalent force distribution in the tensile and compressive areas. For biaxial bending moment, we assume a plastic redistribution of the out-of-plane bending moment between the left and right side of the connection. The M-N curve proposed for out-of-plane bending moment is then applied to each side. The proposed M-N curves fit quite well with numerical results. The comparison to existing experimental tests is also encouraging. In addition a simplified method have been proposed to determine the bending resistance directly related to the axial force and the angle of inclination. The results are quite conservative compared to experimental and numerical one's.

The proposed model assume plastic redistributions of forces between the different components of the connection and thus failure of steel elements excluding failure of concrete components loaded in tension (concrete cone failure...).

REFERENCES

[1] Lescouarc'h, Y., Rigid steel column bases. France: CTICM, 1988 (in French).

[2] DeWolf J.T., Ricker D.T., Column Base Plates, Steel Design Guide Series, AISC, 1991.

[3] EN 1992-4 (Eurocode 2): Design of concrete structures – Part 4: Design of fastenings for use in concrete, Oct 2018.

[4] Jaspart J.P., Vandegans D., Application of the component method to column bases, Journal of Constructional Steel Research, Vol.48, p.89-106, 1998.

[5] Drake R. M., Elkin S. J., Beam-Column Base Plate Design - LRFD Method, Engineering Journal, AISC, Vol. 36, No. 1 (First Quarter), p. 29-38, 1999.

[6] Wald F., Sokol Z., Steenhuis M., Jaspart J.P., Component method for steel column bases, Heron, Vol. 53, p.3-20, 2008.

[7] Stamatopoulos G., Ermopoulos J., Experimental and analytical investigation of steel column bases, Journal of Constructional Steel Research, Vol. 67, p. 1341-1357, 2011.

[8] EN 1993-1-8 (Eurocode 3): Design of steel structures - Part 1-8: Design of joints. Brussels, December 2005.

[9] Fisher J.M., Kloiber L.A., Base plate and anchor rod design, Steel Design Guide Series, AISC, 1991.

[10] Lee D.Y., Goel S., Stojadinovic B., Exposed column-base plate connections bending about weak axis: II. Experimental study, Steel Structures, Vol.8, p. 29–41, 2008.

[11] Lee D.Y., Goel S., Stojadinovic B., Exposed column-base plate connections bending about weak axis: I. Numerical parametric study, Steel Structures, Vol. 8, p. 11–27, 2008.

[12] Bajer M., Vild M., Barnat J., Holomek J., Influence of selected parameters on design optimization of anchor joint, 12th International Conference on Steel, Space and Composite Structures, Prague, 28-30 May 2014, p.149-158, 2014.

[13] Amaral P., Steel column bases under biaxial loading conditions (master degree dissertation). Porto: University of Porto, 2014.

[14] Fasaee M. A. K., Banan M. R., Ghazizadeh S., Capacity of exposed column base connections subjected to uniaxial and biaxial bending moments, Journal of Constructional Steel Research, Vol.148, p. 361–370, 2018.

[15] ECCS, Recommended testing procedures for assessing the behavior of structural elements under cyclic loads, European Convention for Constructional Steelwork, Technical Committee 1, TWG 13 – Seismic Design, No45, 1986.

[16] Packer J., Bruno L., Birkemoe P., Limit analysis of bolted RHS flange plate joints, Journal of Structural Engineering, Vol.115, p.2226-2242, 1989.

[17] Da Silva Seco L., Column base plates under 3D loading, Doctoral thesis, INSA Rennes, 2019.

[18] Da Silva Seco L., Couchaux M., Hjiaj M., Costa Neves L., Column base plates under bi-axial bending moment, Engineering Structures, Accepted under proof, 2020.

[19] European Committee for Standardisation (2004) CEN, Eurocode 2, ENV 1992-1-1:2004, Eurocode 2: Design of concrete structures - Part 1-1: General rules and rules for buildings. Brussels, 2004.

[20] Szczecina M., Winnicki A., Calibration of the CDP model parameters in Abaqus, Advances in Structural Engineering and Mechanics, 2015.

[21] International Federation for Structural Concrete (fib) (2010) FIP Model Code 2010. Lausanne.

Appendix: Results of the parametric study

The initial rotational stiffness, $S_{j,ini}$, ultimate bending moment, $M_{j,u}$, and failure modes are presented from Table A.1 to Table A.6 for the six specimens. Compressive forces are positives (+) and tensile forces negatives (-). The caption code for the failure modes is as follows:

- AB - anchor bolts failure due to tension and bending
- C – column yielding/local buckling due to bending,
- W – weld failure.

Table A.1: *Resistances and failure modes of P1 for M0, M90 and M45*

N (kN)	M0			M90			M45		
	$S_{j,ini}$ (kNm/rad)	$M_{j,u}$ (kNm)	Failure mode	$S_{j,ini}$ (kNm/rad)	$M_{j,u}$ (kNm)	Failure mode	$S_{j,ini}$ (kNm/rad)	$M_{j,u}$ (kNm)	Failure mode
1971	-	-	C	-	-	C	-	-	C
1774	14257	23	C	6068	25	C	23307	27	C
1577	12534	54	C	7419	43	C	17489	43	C
1380	14527	73	C	9061	54	C	15915	65	C
1183	14428	85	C	9383	65	C	13315	79	C
986	13788	97	C	10054	68	C	15414	83	C
788	16316	106	AB	10407	65	C	15250	83	C
591	16541	92	AB	8276	63	C	15644	81	C
394	15120	76	AB	7360	57	C	13653	71	C
197	7212	58	AB	5497	49	C	10303	57	C/W
0	5305	38	AB	3855	34	AB	4945	38	AB
-29	3507	35	AB	2139	31	AB	3068	35	AB
-59	3191	32	AB	1578	28	AB	2638	32	AB
-88	2524	29	AB	1325	26	AB	2101	28	AB
-117	2103	26	AB	1065	23	AB	1938	25	AB
-147	2289	23	AB	916	20	AB	1878	22	AB
-176	1832	20	AB	783	17	AB	1287	17	AB
-205	979	14	AB	539	14	AB	939	13	AB
-235	215	9	AB	73	8	AB	-	7	AB
-264	149	4	AB	64	4	AB	-	3	AB
-293	-	-	AB	-	-	AB	-	-	AB

Table A.2: *Resistances and failure modes of P2 for M0, M90 and M45*

N (kN)	M0			M90			M45		
	$S_{j,ini}$ (kNm/rad)	$M_{j,u}$ (kNm)	Failure mode	$S_{j,ini}$ (kNm/rad)	$M_{j,u}$ (kNm)	Failure mode	$S_{j,ini}$ (kNm/rad)	$M_{j,u}$ (kNm)	Failure mode
1966	-	-	C	-	-	C	-	-	C
1769	14558	44	C	21427	34	C	29844	20	C
1573	19387	62	C	16373	46	C	29847	39	C
1376	15263	74	C	15969	57	C	28512	63	C
1180	17657	89	C	13817	66	C	25110	85	C
983	17171	109	C	12179	78	C	20670	91	C
786	13205	113	AB	10815	81	C	18253	93	C
590	15927	107	AB	8346	76	C	13809	89	C
393	10415	92	AB	8268	68	C	12431	79	C
197	9554	73	AB	6603	60	C	11516	65	C
0	11234	53	AB	5791	46	AB/W	8985	49	AB
-37	5234	48	AB	3303	42	AB	4765	45	AB
-73	4144	43	AB	3023	36	AB	3733	40	AB
-109	3981	37	AB	2290	31	AB	2908	36	AB
-147	3921	32	AB	1760	27	AB	2798	31	AB
-183	2930	26	AB	1560	22	AB	1927	26	AB
-220	551	21	AB	-	18	AB	-	21	AB
-257	411	14	AB	-	12	AB	-	13	AB
-293	-	9	AB	-	7	AB	-	8	AB
-330	-	5	AB	-	3	AB	-	4	AB
-367	-	-	AB	-	-	AB	-	-	AB

Table A.3: *Resistances and failure modes of P3 for M0, M90 and M45*

N (kN)	M0			M90			M45		
	$S_{j,ini}$ (kNm/rad)	$M_{j,u}$ (kNm)	Failure mode	$S_{j,ini}$ (kNm/rad)	$M_{j,u}$ (kNm)	Failure mode	$S_{j,ini}$ (kNm/rad)	$M_{j,u}$ (kNm)	Failure mode
1052	-	-	C	-	-	C	-	-	C
947	7643	22	C	1007	5	C	4666	10	C
842	9000	32	C	1057	10	C	5578	21	C
737	11415	41	C	1109	13	C	6184	29	C
631	10291	55	C	1192	17	C	6256	32	C
526	10979	64	C	1285	18	C	6092	35	C
421	12200	70	AB	1115	19	C	5263	36	AB
316	11737	65	AB	1141	20	C	5990	37	AB
210	10334	56	AB	1380	19	C	5453	36	AB
105	7293	48	AB	1122	18	AB	4571	32	AB
0	4826	41	AB	1141	18	AB	8985	28	AB
-37	4679	37	AB	1049	17	AB	2908	27	AB
-74	3191	34	AB	944	16	AB	2068	24	AB
-110	3174	29	AB	654	13	AB	2209	21	AB
-147	3603	25	AB	450	12	AB	1450	18	AB
-184	3160	21	AB	330	9	AB	978	12	AB
-221	2638	18	AB	228	7	AB	865	8	AB
-257	1680	13	AB	219	5	AB	572	4	AB
-294	1370	8	AB	259	2	AB	532	2	AB
-331	980	3	AB	203	1	AB	274	1	AB
-368	-	-	AB	-	-	AB	-	-	AB

Table A.4: *Resistances and failure modes of P4 for M0, M90 and M45*

N (kN)	M0			M90			M45		
	$S_{j,ini}$ (kNm/rad)	$M_{j,u}$ (kNm)	Failure mode	$S_{j,ini}$ (kNm/rad)	$M_{j,u}$ (kNm)	Failure mode	$S_{j,ini}$ (kNm/rad)	$M_{j,u}$ (kNm)	Failure mode
1062	-	-	C	-	-	C	-	-	C
956	7285	20	C	1182	9	C	4422	10	C
849	11012	31	C	1270	11	C	5605	16	C
743	11242	41	C	1414	15	C	6099	20	C
637	12006	51	C	1153	18	C	6293	29	C
531	12501	65	C	1224	19	C	6632	38	C
425	12233	72	C	1248	19	C	6721	44	C
319	10903	76	AB	1251	20	C	6605	51	AB
212	10691	70	AB	1013	20	C	6226	51	AB
106	10151	62	AB	932	19	C	5566	44	AB
0	7522	51	AB	818	18	C	4894	39	AB
-39	6558	48	AB	667	16	AB	4087	35	AB
-78	5823	44	AB	565	15	AB	3276	32	AB
-116	6028	39	AB	393	15	AB	3411	27	AB
-155	3908	34	AB	304	14	AB	3231	23	AB
-194	2374	29	AB	273	12	AB	2358	19	AB
-233	1931	22	AB	212	10	AB	946	14	AB
-272	1627	15	AB	286	7	AB	786	9	AB
-311	1515	10	AB	372	4	AB	587	4	AB
-349	1314	5	AB	383	2	AB	430	1	AB
-388	-	-	AB	-	-	AB	-	-	AB

Table A.5: *Resistances and failure modes of P5 for M0, M90 and M45*

N (kN)	M0			M90			M45		
	$S_{j,ini}$ (kNm/rad)	$M_{j,u}$ (kNm)	Failure mode	$S_{j,ini}$ (kNm/rad)	$M_{j,u}$ (kNm)	Failure mode	$S_{j,ini}$ (kNm/rad)	$M_{j,u}$ (kNm)	Failure mode
2091	-	-	C	-	-	C	-	-	C
1883	8215	26	C	6431	20	C	11473	22	C
1674	11943	48	C	7533	32	C	12571	37	C
1464	13440	74	C	8139	57	C	14506	62	C
1255	15199	87	C	8852	67	C	16325	75	C
1046	16213	104	C	9745	70	C	15226	80	C
837	17436	111	AB	9981	68	C	15211	80	AB
628	16126	105	AB	11424	67	C	12485	75	AB
418	16728	96	AB	8955	66	C	11446	68	AB
209	10621	80	AB	8793	60	AB	9460	62	AB
0	6442	61	AB	4006	49	AB	6430	52	AB
-55	6001	54	AB	3694	46	AB	5212	48	AB
-109	4971	49	AB	2787	38	AB	4119	40	AB
-164	4158	43	AB	2025	36	AB	3208	35	AB
-218	4183	37	AB	1788	31	AB	2762	27	AB
-273	3271	29	AB	1377	25	AB	1917	23	AB
-327	3095	26	AB	1191	22	AB	-	16	AB
-382	2512	19	AB	-	12	AB	-	13	AB
-436	2694	10	AB	-	9	AB	-	5	AB
-491	-	4	AB	-	2	AB	-	2	AB
-545	-	-	AB	-	-	AB	-	-	AB

Table A.6: *Resistances and failure modes of P6 for M0, M90 and M45*

N (kN)	M0			M90			M45		
	$S_{j,ini}$ (kNm/rad)	$M_{j,u}$ (kNm)	Failure mode	$S_{j,ini}$ (kNm/rad)	$M_{j,u}$ (kNm)	Failure mode	$S_{j,ini}$ (kNm/rad)	$M_{j,u}$ (kNm)	Failure mode
2096	-	-	C	-	-	C	-	-	C
1887	8202	18	C	9941	17	C	11863	19	C
1678	11899	49	C	8848	40	C	10563	49	C
1467	13483	73	C	9194	59	C	12620	68	C
1258	15440	83	C	9075	68	C	14803	84	C
1048	17125	104	C	9886	80	C	13011	96	C
838	18911	117	C	10411	82	C	15854	102	AB
629	17258	122	AB	10402	81	C	15947	101	AB
419	15651	117	AB	9908	78	C	14846	94	AB
209	13507	101	AB	8692	74	AB	11389	83	AB
0	11322	81	AB	6599	64	AB/W	9269	72	AB
-63	9741	75	AB	5046	59	AB	7448	66	AB
-127	8603	68	AB	4737	54	AB	6149	61	AB
-191	8310	62	AB	3784	48	AB	5895	54	AB
-254	6779	53	AB	3464	43	AB	4993	46	AB
-318	5734	45	AB	2424	36	AB	2960	42	AB
-382	2781	34	AB	-	28	AB	1920	31	AB
-445	-	23	AB	-	16	AB	-	22	AB
-509	-	15	AB	-	9	AB	-	15	AB
-572	-	6	AB	-	4	AB	-	6	AB
-635	-	-	AB	-	-	AB	-	-	AB